Kaunas University of Technology

Faculty of Mathematics and Natural Sciences

Molecular Dynamics Investigation of Water Evaporation/Condensation Processes

Master's Final Degree Project

Gediminas Skarbalius

Project author

dr. Algis Džiugys

Supervisor

Kaunas, 2019

Kaunas University of Technology

Faculty of Mathematics and Natural Sciences

Molecular Dynamics Investigation of Water Evaporation/Condensation Processes

Master's Final Degree Project

Applied Physics (6211CX015)

Gediminas Skarbalius

Project author

dr. Algis Džiugys

Supervisor

dr. Teresa Moskaliovienė

Reviewer

Kaunas, 2019

Kauno technologijos universitetas

Matematikos ir gamtos mokslų fakultetas

Gediminas Skarbalius

Vandens garavimo/kondensacijos procesų tyrimas molekulinės dinamikos metodu

Akademinio sąžiningumo deklaracija

Patvirtinu, kad mano, Gedimino Skarbaliaus, baigiamasis projektas tema „Vandens garavimo/kondensacijos procesų tyrimas molekulinės dinamikos metodu“ yra parašytas visiškai savarankiškai ir visi pateikti duomenys ar tyrimų rezultatai yra teisingi ir gauti sąžiningai. Šiame darbe nei viena dalis nėra plagijuota nuo jokių spausdintinių ar internetinių šaltinių, visos kitų šaltinių tiesioginės ir netiesioginės citatos nurodytos literatūros nuorodose. Įstatymų nenumatytų piniginių sumų už šį darbą niekam nesu mokėjęs.

Aš suprantu, kad išaiškėjus nesąžiningumo faktui, man bus taikomos nuobaudos, remiantis Kauno technologijos universitete galiojančia tvarka.

(vardą ir pavardę įrašyti ranka)	(parašas)

Kaunas University of Technology

Faculty of Mathematics and Natural Sciences

Main goal and objectives of final master's thesis

Project tittle	Molecular Dynamics Investigation of Water Evaporation/Condensation Processes
Main goal and objectives	The main goal of the thesis is to investigate the effect of molecular flexibility on liquid-vapour phase change boundary conditions of polyatomic fluids using molecular dynamics simulation method. The main objectives are: • investigate the structure of interphase region, determine the thickness of the interphase layer and liquid-vapour boundaries, which are used to investigate phase-change boundary conditions; • investigate the dependencies of condensation coefficients on properties of liquid and impinging on the interphase vapour molecules and compare obtained results with results from scientific literature, where rigid molecular models of water were used; • investigate motion energy characteristics of reflected molecules; • determine translational velocity distribution functions for evaporation, condensing and reflecting flexible molecules and compare the results with analytical relations from scientific literature.
Supervisor	

Gediminas Skarbalius. Vandens garavimo/kondensacijos procesų tyrimas molekulinės dinamikos metodu. Magistro baigiamasis projektas / vadovas Dr. Algis Džiugys; Kauno technologijos universitetas, Matematikos ir gamtos mokslų fakultetas.

Studijų kryptis ir sritis (studijų krypčių grupė): F300 Fizika, Fiziniai mokslai (Fiziniai mokslai)

Reikšminiai žodžiai: molekulinė dinamika, vanduo, skysčio-garų pusiausvyra, tarpfazinio sluoksnio storis, greičių pasiskirstymas, kondensacijos koeficientas.

Kaunas, 2019. 65 p.

Santrauka

Siekiant nustatyti molekulinio lankstumo įtaką fazinių virsmų kraštinėms sąlygoms, šiame baigiamajame magistro darbe buvo atlikti vandens skysčio-garų pusiausvyros būsenos skaitiniai modeliavimai molekulinės dinamikos metodu. Iš rezultatų matyti, kad dydis, atvirkščias tarpfazinio sluoksnio storiui, yra mažėjanti tiesinė funkcija, priklausanti nuo skysčio temperatūros tirtose temperatūros ribose TIP3P, SPC/E ir flex-FPC molekuliniams vandens modeliams. Kondensacijos koeficientas, gautas naudojant flex-FPC molekulinį modelį, yra skysčio temperatūros ir į skysčio paviršių krentančių molekulių slenkamojo judėjimo energijos komponentės skysčio paviršiaus normalės kryptimi funkcija. Taip pat kondensacijos koeficiento vertės, gautos su flex-FPC molekuliniu modeliu, yra reikšmingai didesnės nei vertės, gautos naudojant SPC/E vandens modelį. Slenkamojo judėjimo energijos komponentės skysčio paviršiaus tangentės kryptimis ir sukamojo judėjimo energija kondensacijos koeficiento vertei įtakos neturi. Iš atsispindėjusių molekulių energijos analizės matyti, kad atsispindėjusių molekulių slenkamojo judėjimo energijos komponenčių skysčio paviršiaus normalės ir tangentės kryptimis ir sukamojo judėjimo energijos pokyčiai tiesiogiai proporcingi atitinkamoms šių energijos komponenčių vertėms prieš molekulės atsispindėjimą. Galiausiai, išgaruojančių, kondensuojančių ir atsispindinčių molekulių greičiai skysčio paviršiaus tangentės kryptimis yra pasiskirstę Maksveliniu pasiskirstymu esant 503 K temperatūrai. Vis dėlto vidutinė išgaruojančių molekulių greičio vertė paviršiaus normalės kryptimi yra didesnė nei vidutinė Maksvelinio pasiskirstymo vertė toje pačioje temperatūroje, o atsispindinčių molekulių greičių pasiskirstymas yra pasislinkęs į mažesnių greičių pusę.

Gediminas Skarbalius. Molecular Dynamics Investigation of Water Evaporation/Condensation processes. Master's Final Degree Project / supervisor Dr. Algis Džiugys; Faculty of Mathematics and Natural Sciences, Kaunas University of Technology. Study field and area (study field group): F300 Physics, Physical science (Physical science)

Keywords: molecular dynamics simulation, water, liquid-vapour equilibria, interphase thickness, velocity distribution, condensation coefficient.

Kaunas, 2019. 65 pages.

Summary

In present master's thesis, molecular dynamics simulations of water liquid-vapour phase equilibria were carried out in order to investigate the effect of molecular flexibility on phase change boundary conditions. The obtained results show that the one over the "10-90" interphase thickness is decreasing linear function of liquid temperature in simulated temperature range for TIP3P, SPC/E and flex-FPC molecular models. The condensation coefficient obtained with flex-FPC molecular model is a function of liquid phase temperature and surface-normal component of translational motion energy of impinging vapour molecule. Furthermore, the condensation coefficients obtained in present master's thesis using flexible molecular model were considerably higher than condensation coefficients obtained with rigid SPC/E molecular model. No dependency of condensation coefficient on surface-tangential components of translational motion energy and rotational energy were observed. The energetic analysis of reflecting molecules showed that changes of surface-normal and surface-tangential components of translational energy and the rotational energy of reflected molecules are proportional to respective energy components of impinging molecules. Finally, the velocity distribution functions of evaporating, condensing and reflecting molecules in surface-tangential directions agree with the Maxwellian distribution at 503 K. However, the mean value of surface-normal component of translational velocity of evaporating molecules is slightly higher than mean velocity obtained from Maxwellian distribution at 503 K temperature and the velocity distribution of reflecting molecules is shifted to lower velocity side.

Contents

Table list

Figure list

Abbreviation list

Abbreviations:

MD – molecular dynamics;

KBC – kinetic boundary conditions;

FPC – fixed-point charge;

TIP3P – transferable intermolecular potential with 3 points;

TIP4P – transferable intermolecular potential with 4 points;

Introduction

The net evaporation and condensation of water are non-equilibrium processes in which molecules cross the interphase region from liquid phase to gas phase and vice versa. The rate of water evaporation and condensation have an influence on the rate of natural water cycle in the nature and have applications in many science and engineering fields, such as physics, chemistry, biology, climatology, astronomy, hydrology, nanotechnology and many more. Therefore, it is important to have accurate and efficient relations with correct boundary conditions for evaluation of phase change rates during evaporation and condensation.

The evaporation/condensation are microscopic processes driven by the molecular collision dynamics at the liquid-vapour interphase. However, in experimental studies, the phase change processes are often considered from macroscopic perspective: the phase change rate is evaluated by mass change rate of the liquid fluid at given fluid and vapour temperatures and pressures. This allows to obtain empirical phase change rates, but it does not provide explanation for the processes at the proximity of the interphase. On the other hand, the theoretical relations, which have been developed to predict the phase change rates (such as Hertz-Knudsen (HK) relation) consider atomistic motion of fluid molecules. The problems arise when the experimental measures often contradict the theoretical predictions and even each another. For example, it was reported that the relative deviation of the experimental rates from the theoretical HK predictions published by many different researchers through the history vary by three orders of magnitude from 0.001 to 1 for case of water. In order to compensate for these the deviations, empirical constants were introduced. However, these constants do not give any explanation for the dynamical processes of fluid molecules at the liquid-vapour interphase and often obscure the problems lying behind theoretical predictions.

The boundary conditions used for phase change relations liquid-vapour interphase (such as HK and HKS relations described above) are often called Kinetic Boundary Conditions (KBC) and the phase change rates is strongly influenced by these conditions. KBC mainly includes the information about number of evaporation events per unit area and unit time and the velocity distribution of liquid surface leaving molecules. KBC also describes evaporation/condensation and thermal accommodation coefficients. The problem is that the boundary conditions often used for rate evaluations might not be entirely correct. It is difficult to experimentally measure velocity distributions of evaporating and condensing molecules. However, it is often assumed that molecules leaving the surface and impinging on it are distributed by the Maxwellian velocity distribution, whereas the evaporation is a non-equilibrium process and the Maxwellian distribution holds only for equilibrium states. Secondly, there exists few molecular diameters thick temperature and pressure discontinuities at the liquid-vapour interphase layers (which are called temperature jumps) of the evaporating liquid which are also challenging to measure experimentally. As a consequence, the boundary conditions for phase change relation obtained by measuring the temperature of bulk liquid and vapour phases might not be correct boundary conditions at the molecular levels. A method which provides possibility to investigate these boundary conditions on molecular level and without any uncertainty is Molecular Dynamics (MD) simulations.

In previous molecular dynamics studies of phase change boundary conditions, the main object of the research was monoatomic or simple rigid polyatomic fluids. However, the research on flexibility effect on these boundary conditions are lacking even though it is property of polyatomic molecules. The main **goal** of the present master's thesis is to investigate the effect of molecular flexibility on

liquid-vapour phase change boundary conditions (such as velocity distributions of evaporation/condensing molecule, condensation/evaporation coefficients etc.) of polyatomic fluids using molecular dynamics simulation method. In this master's thesis, simulations were performed using flexible molecular model of water, which includes harmonic OH bonds and HOH angle vibrations. Water was chosen due to its relatively simple geometric structure and presence of comparable information on the boundary conditions obtained with rigid models. The main **objectives** on the master's thesis are:

- investigate the structure of interphase region, determine the thickness of the interphase layer and liquid-vapour boundaries, which are used to investigate phase-change boundary conditions;
- investigate the dependencies of condensation coefficients on properties of liquid and impinging on the interphase vapour molecules and compare obtained results with results from scientific literature, where rigid molecular models of water were used;
- investigate motion energy characteristics of reflected molecules;
- determine translational velocity distribution functions for evaporation, condensing and reflecting flexible molecules and compare the results with analytical relations from scientific literature.

1. Literature review

The net evaporation and condensation of water are non-equilibrium processes in which molecules cross the interphase region from liquid phase to gas phase and vice versa. The rate of water evaporation and condensation have an influence on the rate of natural water cycle in the nature and have applications in many science and engineering fields, such as physics, chemistry, biology, climatology, astronomy, hydrology, nanotechnology and many more [1],[2],[3]. Therefore, it is important to have accurate and efficient relations with correct boundary conditions for evaluation of phase change rates during evaporation and condensation.

The evaporation/condensation are microscopic processes driven by the molecular collision dynamics at the liquid-vapour interphase. However, in experimental studies, the phase change processes are often considered from macroscopic perspective: the phase change rate is evaluated by mass change rate of the liquid fluid at given fluid and vapour temperatures and pressures. This allows to obtain empirical phase change rates, but it does not provide explanation for the processes at the proximity of the interphase. On the other hand, the theoretical relations, which have been developed to predict the phase change rates (such as Hertz-Knudsen (HK) relation) consider atomistic motion of fluid molecules. The problems arise when the experimental measures often contradict the theoretical predictions and even each another. For example, it was reported by the recent review paper that the relative deviation of the experimental rates from the theoretical HK predictions published by many different researchers through the history vary by three orders of magnitude from 0.001 to 1 for case of water [4]. In order to compensate for these the deviations, empirical constants were introduced. However, these constants do not give any explanation for the dynamical processes of fluid molecules at the liquid-vapour interphase and often obscure the problems lying behind theoretical predictions.

In this section, the theoretical relations used for liquid-vapour phase change rate evaluation will be introduced with assumptions and boundary conditions used to derive these relations. Then, the review of scientific literature on MD simulation studies considering the liquid-vapour phase change boundary conditions for various monoatomic and polyatomic molecular fluids will be presented. Finally, the main goal and tasks of the master's thesis will be formulated considering the scientific work that has been already done in this field.

1.1. Knudsen relation

Two widely used relations in scientific literature which allows to evaluate the phase change rate between liquid and vapour phases during net evaporation/condensation are HK relation and Schrage relations [5]. Both of the relations were derived from kinetic theory of gases by counting the number of molecules crossing unit area per unit time in vapour phase assuming that vapour molecules are distributed according to Maxwellian velocity distribution. The main difference between these relations is that Schrage relation accounts for bulk vapour motion which is induced by the evaporation/condensation flux of the fluid.

The HK relation has many different forms in various scientific sources. For example, HK relation is sometimes given in form where the driving "force" of phase change is a difference in the liquid and vapour temperatures at the interphase region [6]. Other times, it is assumed that there is a thermodynamic equilibrium between liquid and vapour, which means that the liquid and vapour temperature is equal and the driving force is the difference in saturation and vapour pressures [7]. Furthermore, the empirical coefficients are often introduced to HK relation in order to explain the

deviation from the experimental values. These coefficients are called evaporation and condensation coefficients. The meaning of these coefficients will be explained bellow.

The HK relation can be derived by, firstly, assuming that the vapour phase is ideal gases, which are in thermodynamic equilibrium with its liquid (vapour is saturated). Then, the velocity distribution of vapour phase molecules can be assumed to be Maxwellian. In this case, the mean velocity of molecular motion in vapour phase is simply given by

$$\bar{v} = \sqrt{\frac{8k_B T_e}{\pi m}} \tag{1}$$

where k_B is the Boltzmann, T_e is the vapour temperature at the equilibrium and m is the mass of the vapour molecule. The number of molecules that cross unit area per unit time in vapour is given by [8]

$$J_N = \frac{1}{4} n\bar{v} \tag{2}$$

where n is the molecular number density. According to ideal gas law and equations (1) and (2), the theoretical mass flux consisting of vapour molecules crossing the interphase is given

$$J_e^V = J_N m = p_s(T_e)\sqrt{\frac{m}{2\pi k_B T_e}} \tag{3}$$

where p_s is the pressure of saturated vapour at the flat interphase. The superscript "V" indicates the vapour phase and subscript "e" indicates that the flux is at liquid-vapour equilibrium.

At liquid-vapour equilibrium, the net mass transfer between two phases is equal to zero. This means that the mass flux consisting of the vapour molecules traveling through the interphase J_e^V is equal to the mass flux consisting of the liquid molecules traveling through the interphase J_e^L. Furthermore, mass flux J_e^L is the theoretical maximum mass flux which depends only on liquid temperature and is independent of vapour phase temperature or pressure. At net evaporation or condensation conditions, the vapour pressure is deviated from saturation pressure and, as a consequence, the flux J_e^V is not equal to J_e^L. However, flux J_e^L stays the same at given liquid temperature. Therefore, the mass flux J during net evaporation/condensation is given by

$$J = J^L + J^V = J_e^V - J^V = p_s(T_I^L)\sqrt{\frac{m}{2\pi k_B T_I^L}} - p_I^V\sqrt{\frac{m}{2\pi k_B T_I^V}} \tag{4}$$

where subscript "I" indicates the interphase region. The "-" sign appears because these fluxes are antiparallel. The idealized control volume at the interphase is given in Fig. 1 and Eq. (4) is Knudsen relation.

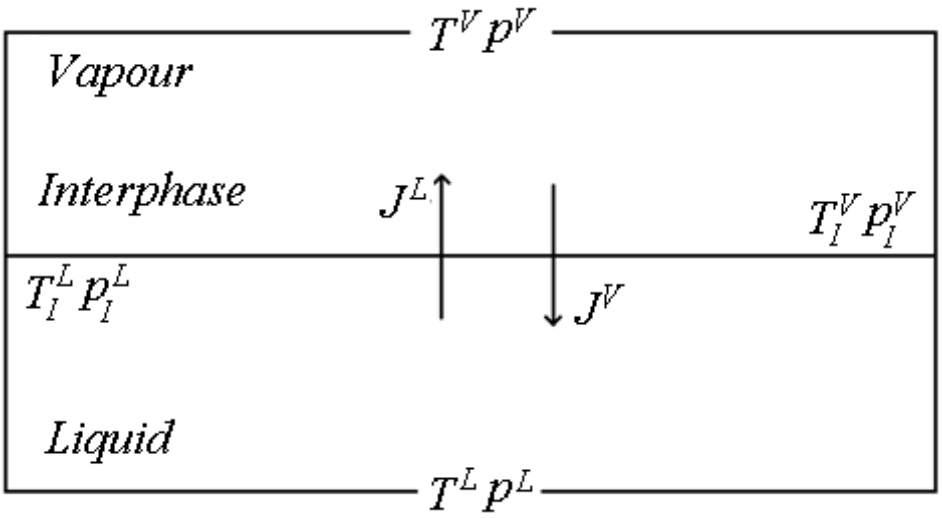

Fig. 1. Idealized control volume at liquid-vapour interphase during evaporation and condensation. This figure was adopted from [9].

1.2. Empirical coefficients and Hertz-Knudsen-Schrage relation

It was noticed that eq. (4) often predicts greater phase change rates than experimentally measured ones. It was argued that the reason for it is that not every liquid or vapour molecule that enters the interphase changes its phase: part of vapour molecules reflect of the interphase and part of liquid molecules return into liquid phase. Therefore, there was a need for coefficients to account for occurrences. These coefficients are evaporation coefficient σ_e and condensation coefficient σ_c. Then, the eq. (4) can be written as

$$J = \sigma_e p_s(T_I^L) \sqrt{\frac{m}{2\pi k_B T_I^L}} - \sigma_c p_I^V \sqrt{\frac{m}{2\pi k_B T_I^V}} \tag{5}$$

Eq. (4) is called Hertz-Knudsen relation [4]. The condensation coefficient (also sometimes called a mass accommodation coefficient) is defined as the probability of vapour molecule to join the liquid phase when it impinges on the interphase without thermal emission of any other particle [10]. Analogically, the evaporation coefficient is defined as the probability of liquid molecule to leave the liquid phase when it enters interphase. In other words, these coefficients define the ratios of the measured mass fluxes at the surface to theoretical maximum mass fluxes from kinetic theory of gases. Respectively, the value of these coefficients is between 0 and 1.

It is worth noticing, that when values of J, T_I^L T_I^V and p_I^V are evaluated experimentally, there are still two unknowns σ_e and σ_c which cannot be determined simultaneously. Therefore, it is necessary to use simplifying assumptions before applying the eq. (5). Other authors include additional heat and momentum equations in order to describe heat and mass transfer in closed systems [9]. Furthermore, experimental investigation exclusively on σ_e and σ_c is extremely complex.

Later on, it was claimed by Schrage, that the molecular velocity distribution deviates from Maxwellian during net evaporation/condensation and it should be shifted by the mean drift velocity of vapour bulk [4]. Then, the modified relation for net mass flux is given by

$$J = \frac{2}{2-\sigma_c}\sqrt{\frac{m}{2\pi k_B}}\left[\frac{\sigma_e p_s(T_I^L)}{\sqrt{T_I^L}} - \frac{\sigma_e p_I^V}{\sqrt{T_I^V}}\right] \quad (6)$$

Eq. (6) is called Hertz-Knudsen-Schrage (HKS) relation. It is worth noticing that mass the flux is equal to doubled value of mass flux from HK relation when the coefficients are equal to 1.

1.3. Thermal accommodation coefficient

Only σ_c part of molecules impinging on the interphase condenses. However, the other part $(1-\sigma_c)$ is reflected back to the liquid phase. There are two mechanisms by which molecules are reflected back into vapour phase [11]: specular reflection and diffusive reflection. During the specular reflection, the molecule does not interreact with the surface thermally which means that its kinetic energy after reflection is the same as before reflection. In the case of diffusive reflection, molecule is thermally accommodated to the surface and the kinetic energy after reflection changes, i.e. molecules reflect with surface temperature. The coefficient which describes the thermal interaction of reflected molecules with the interphase is called thermal accommodation coefficient and is defined as [12], [13]:

$$\alpha_t = \frac{(E_2 - E_1)}{(E_I - E_1)} \quad (7)$$

where E_1 and E_2 are the kinetic energies of molecules before and after reflection and E_I is the energy of interphase (or surface) molecules. Sometimes, a temperature of molecules is used to define α_t [14]. As in the case of evaporation/condensation coefficients, the value of α_t is between 0 and 1. The α_t part of reflected molecules experiences specular reflection and $(1-\alpha_t)$ of reflected molecules experience diffusive reflection.

1.4. Kinetic boundary conditions in liquid-vapour phase change relations

The boundary conditions used for phase change relations liquid-vapour interphase (such as HK and HKS relations described above) are often called Kinetic Boundary Conditions (KBC) and the phase change rates is strongly influenced by these conditions. KBC mainly includes the information about numbers of evaporation events per unit area and unit time and the velocity distributions of liquid surface leaving molecules. KBC also describes evaporation/condensation and thermal accommodation coefficients.

The problem is that the boundary conditions often used for rate evaluations might not be entirely correct. It is difficult to experimentally measure velocity distributions of evaporating and condensing molecules. However, it is often assumed that molecules leaving the surface and impinging on it are distributed by the Maxwellian velocity distribution, whereas the evaporation is a non-equilibrium process and the Maxwellian distribution holds only for equilibrium states [9]. Secondly, there exists few molecular diameters thick temperature and pressure discontinuities at the liquid-vapour interphase layers (which are called temperature jumps) of the evaporating liquid which are also challenging to measure experimentally[4], [15]. As a consequence, the boundary conditions for phase change relation obtained by measuring the temperature of bulk liquid and vapour phases might not be correct boundary conditions at the interphase layers at molecular levels. A method which provides possibility to investigate these boundary conditions on molecular level and without any uncertainty is Molecular Dynamics (MD) simulations.

1.5. Review on the molecular dynamic studies on liquid-vapour phase change boundary conditions

The liquid-vapour equilibrium molecular dynamics simulations were performed by Nagayama et al. in work [16], in order to investigate evaporation/condensation processes of liquid argon at five different temperatures: 84 K, 90 K, 102 K, 120 K and 130 K. Authors simulated thin liquid argon film placed in the of the z axis of the simulation box (liquid surface normal is parallel with the z axis) with periodic boundary conditions along x, y and z axis. System configuration in xz plane is given in Fig. 2. The total number of molecules (although argon is atomic fluid, it will be considered as monatomic molecular fluid) is 864 for 84-120 K cases and 1728 for 130 K case. The interaction between molecules was described by well-known Lennard-Jones (LJ) pairwise intermolecular potential with argon parameters. Authors defined condensation coefficient as the ratio of number of condensed molecules N_c to the number of all impinging on the surface molecules N_{all}, which is a sum of number of condensed molecules N_c and number of reflected molecules N_r:

$$\sigma_c = \frac{N_c}{N_{all}} = \frac{N_c}{N_c + N_r} \tag{8}$$

It was concluded that condensation coefficient for monoatomic fluids is a function of liquid surface temperature and surface-normal component of kinetic energy of translational motion and can be expressed as:

$$\sigma_c = \alpha \left[1 - \beta \exp\left(-\frac{E_z}{k_B T}\right)\right] \tag{9}$$

where α and β are constants, which are determined by regression analysis for each case. However, the analysis of impact of tangential velocities of atoms on condensation coefficients were not performed. The macroscopic condensation coefficient, which is the mean value of microscopic energy dependent coefficient given by eq. (9), was obtained to be decreasing function of temperature. Furthermore, authors showed that the tangential and surface-normal components of all surface leaving molecules, including evaporated and reflected molecules are distributed according to the Maxwellian distribution. However, the velocity distributions calculated separately for evaporated and reflected molecules show deviation from the Maxwellian. The mean kinetic energy of reflected molecules was lower than Maxwellian mean energy at given temperature. Therefore, authors suggested modifications for Maxwellian distribution including α and β constants obtained from condensation coefficient calculations in order to give better agreement with simulation results:

$$F_{z,e}(v_z) = \frac{1 - \beta \exp(-m v_z^2/(2k_B T))}{1 - \beta/2} \left(\frac{m}{k_B T}\right) v_z \exp\left(-\frac{m v_z^2}{2k_B T}\right) \tag{10}$$

for evaporation and

$$F_{z,r}(v_z) = \frac{1 - \alpha + \alpha\beta \exp(-m v_z^2/(2k_B T))}{1 - \alpha + \alpha\beta/2} \left(\frac{m}{k_B T}\right) v_z \exp\left(-\frac{m v_z^2}{2k_B T}\right) \tag{11}$$

for reflection. They also showed that argon atoms with low surface-normal and surface-tangential components of translational energy tend to be reflected with higher translational energy and the ones

with higher energy tend to transfer part of their kinetic energy to the liquid surface during the reflection.

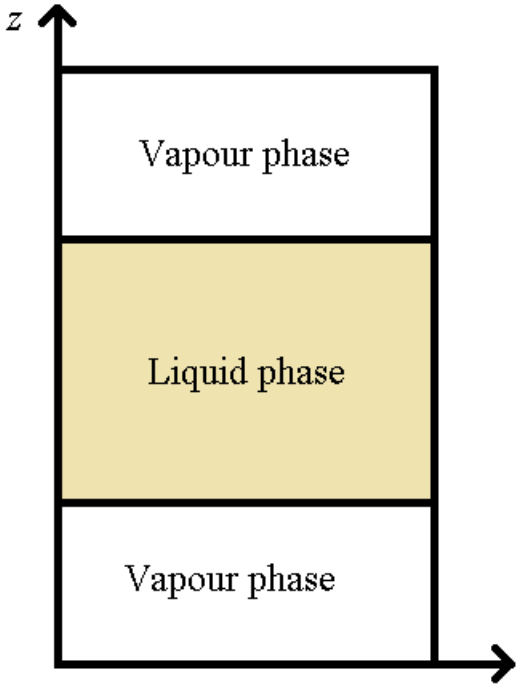

Fig. 2. Projection of simulation system in xz plane, which was used to study evaporation/condensation processes at liquid-vapour phase equilibrium in work [16]. The thin liquid argon film is placed in the simulation box with boundary conditions in x, y and z axis.

Nagayama et al. carried out the evaporation/condensation investigation on typical polyatomic fluid (water) in work [17], where same simulation methodology was used as in argon case. In this work, authors simulated water film using rigid SPC/E molecular models at eight different temperatures: 330 K, 373 K, 390 K, 450 K, 474 K, 500 K, 515 K and 550 K. The number of water molecules used for all temperature cases is 1024. In lower temperature cases where number of evaporation evens were relatively low, authors used method where molecules were inserted into vapour phase with random velocities from Maxwellian distribution towards the surface. Authors showed that molecular exchange phenomenon, during which the condensation event of molecule is followed by thermal emission of other surface molecules, has no significant effect on condensation process of water. They also showed that condensation coefficient of polyatomic fluids is also a function of kinetic energy of translational motion in surface-normal direction and surface temperature and can be expressed by Eq. (9), as in case of monoatomic molecules. Furthermore, authors claimed that no effects of incident angle, surface-tangential component of translational motion energy and rotational motion energy on condensation coefficient were noticed. They also stated that the reason for small values of condensation coefficient is that there exist constraints of translational motion for molecules at the interphase, which occurs due to nonhomogeneous potential field.

Unique way to determine evaporation/condensation coefficient was proposed by Yang et al. in their works [15] and [18], where molecular dynamics simulation study of water thin film evaporation using

rigid TIP4P molecular model at temperatures: 363 K, 383 K, 403 K, 423 K, 443 K and 463 K was presented. Simulations were performed in same configuration as given in Fig. 2. Authors showed that mean temperature at the interphase region was lower by approximately 5 K than the liquid temperate during evaporation. They explained that the temperature difference at the interphase occurs because evaporation takes place when more energetic molecules leave the interphase and, therefore, the mean kinetic energy as well as the temperature of interphase is lower. Also, authors presented a relation for evaporation coefficient evaluation, which was derived by combining HKS relation with the molecular dynamics simulations. Their evaluation of evaporation coefficient is given by

$$\sigma_e = \frac{C_1 C_2}{\left(\frac{A_I}{V}\right)\left(\frac{M}{2\pi R}\right)^{\frac{1}{2}} \frac{p_L}{T_L^{1/2}}} \tag{12}$$

where A_I is area of the interphase, V is the volume of vapour side, M is the molar mass, R is the universal gas constant, p_L is the saturation pressure at the interphase and T_L is the temperature of the interphase. Constants C_1 and C_2 are determined from the simulation results by fitting a molecular number density evolution function in time, which is given by

$$n(t) = C_1(1 - \exp(-C_2 t)) \tag{13}$$

Evaporation coefficients obtained by eq. (13) in this work increases with rising temperature. However, there are few problems related with performed simulations. Firstly, this expression was derived assuming that evaporation coefficient is equal to condensation coefficient before equilibrium state is reached in simulation, which might not be correct in non-equilibrium states. Secondly, the derived relation suggests that the evaporation coefficient might be dependent on the dimensions of the simulation domain, but the system size sensitivity analysis was not performed. Finally, the dimensions of vapour phase region in every direction is lower or close to the mean free path of water molecules in vapour phase at given temperatures, which means that most of the molecules travel through the vapour region without interacting with other vapour molecules until it condenses on the other side of the liquid film.

In work [13], Nagayama et al. performed non-equilibrium molecular dynamics and Monte Carlo simulations in order to study inverse temperature profiles (the phenomena where the heat flux in opposite direction of the condensation flux occurs near the condensing surface) during steady evaporation state of argon. A constant non-equilibrium condition was obtained by two thermostats which maintained two sides of liquid at different temperatures ($T_H > T_L$) as shown in Fig. 3 (in MD, thermostat is a method applied in simulations, which allows to control temperature of certain groups of molecules and/or temperature in certain regions). In given configuration, evaporation takes place at lower interphase and condensation takes place at the upper interphase.

Authors also proposed new definition for accommodation coefficient:

$$\alpha_t = \frac{(E_1 - E_2)}{(E_1 - E_s)} \tag{14}$$

and

$$E_s = \int_0^{\infty} \frac{1}{2} m v_z^2 F_{z,r} dv_z = \frac{1-\alpha+\alpha\beta/4}{1-\alpha+\alpha\beta/2} k_B T \tag{15}$$

where E_1 is the energy of the molecule before reflection from the surface, E_2 is the energy of the molecule after reflection and E_s is the energy of reflected molecule if they were completely accommodated to the surface. Parameters α and β are taken from Eq. (9). With this definition of E_s, it is accounted that the mean energy of reflected molecules is lower than mean energy of molecules at liquid surface. Authors found, that the accommodation coefficient decreases when the molecular mass flux near the condensing surface increases. Authors also obtained inverse temperature profile at the condensing interphase. Explanation for obtained inverse profile is the accumulation of excess energy of reflected molecules, which occurs due to low value of accommodation coefficient. The temperature jump at the interphase increases with increasing difference in bulk liquid and vapour phase temperatures. They also proposed modified boundary conditions for reflected molecules during net condensations, which accounts for the temperature change due to the temperature jump:

$$F_{z,r} = \frac{1-\alpha+\alpha\beta \exp\left(-\frac{m v_z^2}{2 k_B T'}\right)}{1-\alpha+\alpha\beta/2} \left(\frac{m}{k_B T'}\right) v_z \exp\left(-\frac{m v_z^2}{2 k_B T'}\right) \tag{16}$$

Where T' is the modified temperature of the condensing interphase, which is the function of accommodation coefficient and molecular mass flux.

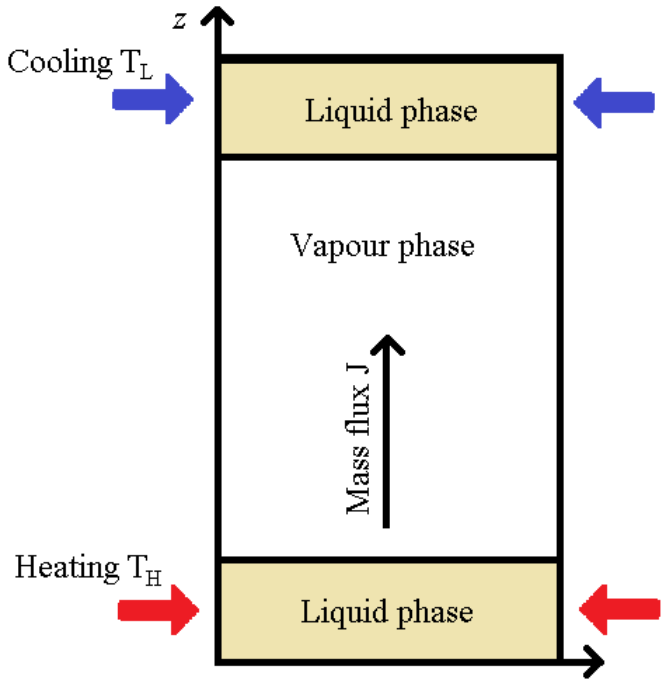

Fig. 3. Projection of simulation system in xz plane, which was used to study evaporation/condensation processes at non-equilibrium conditions in paper [13]. The thin liquid argon film is placed in the simulation box with boundary conditions in x, y and z axis. Evaporation is induced by two thermostats, which maintain two sides of liquid film at different temperatures.

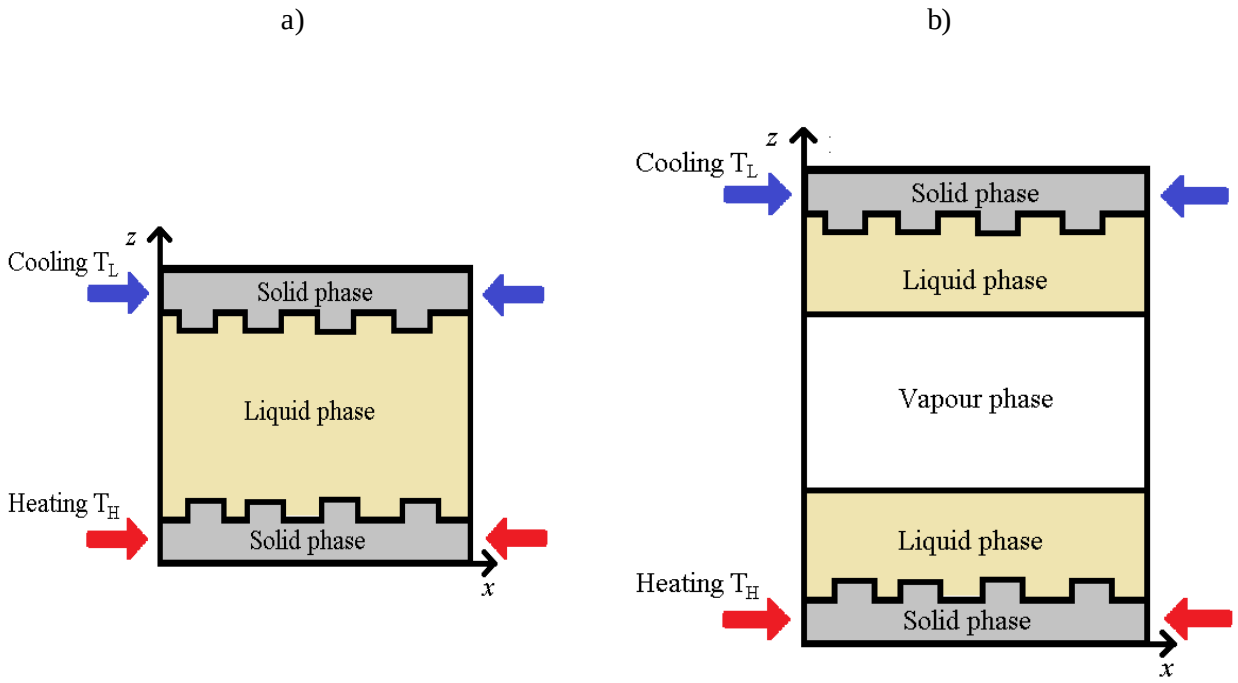

Fig. 4. Projection of simulation systems in xz plane, which was used to study evaporation/condensation processes of liquid argon contained in nanostructured channels in works [19] and [20]: a) simulation without vapour phase; b) simulation with vapour phase. Periodic boundary conditions are applied in x, y and z axis for both cases.

In works [19] and [20], Nagayama et al. performed molecular dynamics simulations of argon confined by two platinum nanostructured plates in order to investigate the effects of nanostructures on evaporation rates. Interaction between molecules were described by modified LJ potential which provides possibility to change solid surface wettability. The two types of simulations were performed. In the first type, the void between two platinum plates was fully filled with liquid argon (see Fig. 4 a)). There exist only two solid-liquid interphases and there is no phase change in the system. In the second type simulations, the void is partially filled with two liquid films on both platinum plates with additional space for the vapour phase in the middle of the z axis: there exists two solid-liquid and two liquid-vapour interphases in the system (see Fig. 4 b)). In first type of simulation, the size of simulation box in z axis is 7.22 nm and the distance between the platinum plates ranges from 3.6 nm to 5.41 nm. In second type of simulations, the size of simulation box in z axis is increased to 12.62 nm. In both cases one of the platinum wall is cooling wall and the other one is heating wall i.e. there exists steady heat and mass fluxes during the simulations. Simulations were performed with both flat solid walls and solid walls with added nanostructures. These structures were described by parameter r_w which is the ratio of flat wall area to nanostructured wall area. It was found that there exist temperature jumps at solid-liquid interphase. These temperature jumps obtained for hydrophobic surfaces are higher than in hydrophilic surface cases. From temperature gradients and existing heat fluxes in the system, authors found that thermal conductivity of nanostructured surfaces is greater than thermal conductivity of flat surfaces, which means that lower thermal resistance can be achieved by adding nanostructures to the contact surface with liquid. Furthermore, it was found that the evaporation rate is constant from 0 ns to 2 ns with average value of around 828 kg/m^2. In this stage, the nanostructures on the solid surface do not have significant effect. In later stage from 2 ns to 5 ns the evaporation rate starts to decrease due to fluid interaction with the solid. After 5 ns, only absorbed

layer is left and total evaporation flux comes down to zero. However, the mean evaporation flux with flat solid surfaces were 466 kg/m^2. Authors concluded that nanostructures might help increase the evaporation rates of thin liquid films due to better heat transfer from the solid phase to the liquid phase.

MD studies of phase change boundary conditions of monoatomic and simple polyatomic fluids were extended to fluids consisting of chain molecules by Nagayama et al. in work [21], where structure and thermodynamic properties as well as evaporation/condensation coefficients of three different length straight-chain alkane group molecules: butane, octane and dodecane were examined. System configuration used in these simulations is same as the one given in Fig. 2. The intramolecular interactions of molecular chains were described by AMBER force field. Butane simulations were carried out in 220 K, 300 K and 340 K, Octane – in 330 K, 430 K and 460 K and dodecane – in 300 K, 500 K and 550 K temperatures. It was found, that just like in case of monoatomic and simple polyatomic fluids, the condensation coefficient of chain molecules also depends on energy of translational motion in surface-normal direction and surface temperature and obeys eq. (9). The probability densities of orientation parameter for evaporation and condensing molecules were examined showing that the orientation of molecules slightly depends on length of the molecule. Furthermore, it was shown that no significant effect of chain molecule orientation on condensation coefficient was found.

KBCs of argon at liquid-vapour interphase were examined using MD simulations by Fujikawa et al. in work [22]. Simulation were performed in temperature interval from 85 K to 130 K. In this work, evaporation and condensation coefficients were using mass fluxes:

$$\sigma_e = \frac{\langle J_{evap}^{sp} \rangle}{\langle J_{out} \rangle_e} = \frac{\langle J_{evap}^{sp} \rangle}{\langle J_{evap}^{sp} \rangle + \langle J_{ref} \rangle} \tag{17}$$

and

$$\sigma_c = \frac{\langle J_{cond} \rangle}{\langle J_{coll} \rangle} = \frac{\langle J_{cond} \rangle}{\langle J_{cond} \rangle + \langle J_{ref} \rangle} \tag{18}$$

where $\langle J_{evap}^{sp} \rangle$ is the mean mass flux of spontaneously evaporating molecules, which depends only on surface temperature, $\langle J_{cond} \rangle$ is the mean mass flux of condensing molecules, $\langle J_{ref} \rangle$ is the mean mass flux of reflected molecules, $\langle J_{out} \rangle_e$ is the mean mass flux of outgoing from the surface molecules at equilibrium, which is sum of $\langle J_{evap}^{sp} \rangle$ and $\langle J_{ref} \rangle$ and, finally, $\langle J_{coll} \rangle$ is the mean mass flux of vapour molecules, which undergo collisions with the interphase: $\langle J_{coll} \rangle = \langle J_{cond} \rangle + \langle J_{ref} \rangle$. The value of $\langle J_{evap}^{sp} \rangle$ is obtained by so-called virtual vacuum simulations, where evaporated molecules are deleted from the system and there is no mass flux towards the liquid surface. Authors found, that evaporation/condensation coefficients (defined by equations (17) and (18)) is close to 1 below triple point temperature and is decreasing function of liquid temperature. Authors also examined the velocity distributions of argon molecules evaporating into virtual vacuum and showed that velocity distributions agree with half-Maxwellian distributions except for high temperature cases.

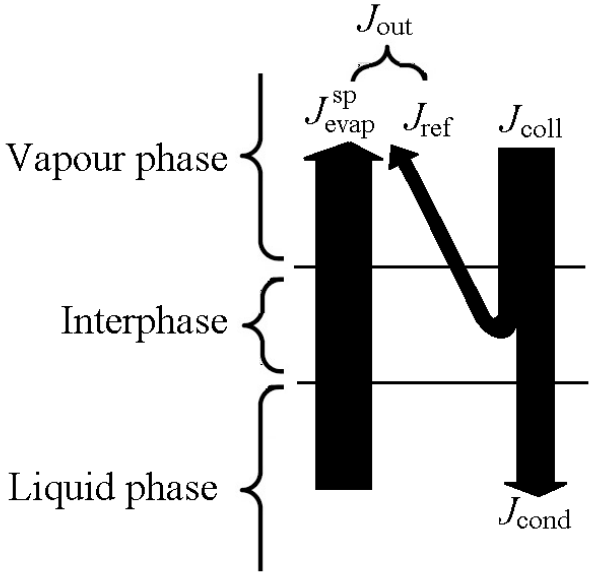

Fig. 5. Mass fluxes through the interphase region. This figure was adopted from [22].

Fujikawa et al. extended their previous KBC study to methanol and water - typical polyatomic fluids in works [23] and [24], where authors performed MD simulation liquid-vapour equilibria and steady evaporation into virtual vacuum. Water was simulated in temperature interval from 300 K to 460 K and methanol – in temperature range from 260 K to 390 K. Water was simulated using TIP3P force field model and methanol was simulated using OPLS force field model. Evaporation/condensation coefficients were defined in same way as in the previous study (equations (17) and (18)). Just like in argon case, the condensation coefficient of methanol and water is close to 1 at lower temperatures and is decreasing function of liquid phase temperature. Furthermore, translational and rotational velocity distributions of water and methanol molecules evaporating into virtual vacuum were determined. For both water and methanol cases, it was found that the translational velocity distribution agrees with half-Maxwellian distribution except for higher temperatures and velocity distribution of rotational motion also agrees with Maxwellian distribution at given temperatures.

More recent MD study on argon kinetic boundary conditions was performed by Watanabe et al. in work [25], where authors performed thin argon film evaporation simulations in liquid-vapour equilibrium at 85 K. In this study, authors used two-boundary method to evaluate evaporation events. One boundary was place in liquid phase, which is called liquid boundary. Other one is placed in vapour phase, which is called vapour boundary. Molecular events at the surface is captured when molecules cross these boundaries. Furthermore, authors suggested a unambiguous way to determine the positions of liquid and vapour boundaries. This evaporation event counting method will be described in more detail in methodology section as it was used in present work. Authors showed that the velocity distribution of the surface-normal component of evaporating molecules coincide with the Maxwellian distribution at the liquid temperature, which agrees with previous studies. However, the mean velocity is slightly higher than the prediction from Maxwellian. The velocity distributions of reflecting and before reflection molecules are shifted towards the lower temperatures and the mean velocity are lower than Maxwellian mean at the liquid temperature. Authors also proposed the way

to describe the velocity distribution of all surface leaving molecules from evaporating and reflecting molecules velocity distributions incorporating the definitions of evaporation and condensation coefficients. Another works of Watanabe et al. concerning the examination of kinetic boundary conditions using simulations based on mean-field kinetic theory are [26] and [27].

In following works based on MD [28] and [29], Watanabe et al. performed MD simulations of the liquid-vapour equilibrium of binary mixture in order to study on KBCs of binary mixtures and the influence of non-condensable gases. Simulations were performed at two different temperatures 85 K and 95 K. Binary gas mixture consisted of argon, which was considered as condensable vapour and neon, which was considered as non-condensable gas. Molar fraction of gas in the mixture ϕ varied from 0 to 0.032, where ϕ is defined as

$$\phi = \frac{N_G}{N_V + N_G} \tag{19}$$

N_g is the number of gas molecules in the system and N_V is number of vapour molecules in system. Simulation configuration is the same as given in Fig. 2 and the total number of molecules in the system was 6000 in all cases. Argon and neon molecules interacted via LJ pairwise potential. Evaporation even counting was done using same method as in their previous study. Authors found that the surface-normal component of translational velocity for evaporated vapour molecules is distributed according to Maxwellian distribution with slightly higher mean velocity for all values of ϕ.The mean velocity of reflected molecules, however, is lower than Maxwellian. In a case of gas molecules, velocity distributions of both evaporated and reflected molecules are in agreement with Maxwellian distribution. Furthermore, from mass fluxes at the interphase, authors examined evaporation/condensation coefficients for vapour and non-condensable gases. Obtained evaporation and condensation coefficients for both vapour and gas are equal at equilibrium state and decreasing function of gas molar fraction in the system ϕ. The coefficient values for argon is significantly higher than for neon.

In the work [30] Julin et al. were concerned with temperatures more related with condensational growth of sub-micrometre water particles in the atmosphere. Therefore, they carried out MD simulations of water evaporation and condensation from thin water films and droplets with different radii values of 1.92 nm and 4.14 nm in temperature range from 268 K to 300 K using TIP4P-Ew molecular model. There were two types of simulations performed: evaporation simulations, which were carried out to determine evaporation rates into vacuum and mass accommodation simulations, which were carried out to investigate mass accommodation coefficients. In evaporation simulations, authors did not use real vacuum conditions, which means that evaporated molecules were to travel in the vapour phase and to return into other side of the liquid phase. Authors argued that due to a small number of evaporation evens and only a few molecules in vapour phase at simulated temperatures, these simulations are good approximation of vacuum conditions. In mass accommodation simulations, authors used similar approach as in [17], where molecules were inserted in vapour phase with initial velocities taken from Maxwellian distribution. In thin film cases molecules were inserted in both sides of the film with random coordinates in xy plane with initial velocities towards the surface. For the droplet cases, the incident molecules were placed in random location of simulation domain with velocities towards the centre of mass of the droplet. Each case had 1000 incident molecules. Obtained evaporation rates in the simulations were compared with theoretical predictions from kinetic theory of gases. It was found that theoretical evaporation rates predicted by kinetic theory

of gases were in an agreement with simulation results when saturation pressures from MD simulation was used while evaporation rates were overestimated when actual experimental saturation pressures were used. It was noticed that the evaporation rates in mass accommodation simulations were slightly higher than the rates from evaporation simulations, which is a consequence of molecular exchange process. This finding contradicts the assumption that the evaporation mass flux is independent of molecular collision rate of the vapour molecules with the surface. Furthermore, authors found that the mass accommodation coefficient is close to unity in all studied temperatures. The coefficient slightly decreases as the temperature increases. Furthermore, when molecular exchange is considered, the mass accommodation coefficient decreases slightly faster as temperature increases in given temperature range. However, the value is close to unity as well and there is no significant difference. Lastly, the mass accommodation coefficient slowly increases as the radius of the droplet increases.

In the work [31], MD simulations were performed in order to find the parameter values of SPC/E based water model which reproduces the previously obtained experimental evaporation and condensation coefficients at 300 K. Authors argued that if these experimental coefficients are correct, then there should exist molecular models which reproduces same condensation coefficients at these conditions. Modified parameters in water model was the dipole moment of water molecule and LJ potential parameters. Authors stated, that the dipole moment of water molecule in liquid is 2.35 D and vapour phase molecules have dipole moment of 1.85 D, therefore, the dipole moment of the condensing molecule should be reduced, which decreases the possibility for vapour molecules to form hydrogen bonds and reduces the probability to be accommodated to surface. Authors also argued that during condensation processes some of translational energy of molecules might be transferred to OH bond and HOH angle vibrations. Therefore, artificial harmonic force constants were added to the model, i.e. molecular flexibility was introduced to the molecule. Simulations were performed by randomly inserting modified molecule into vapour phase with velocities from Maxwellian distribution towards liquid surface, which consists of non-modified molecules. Authors found that the condensation coefficient decreases as the dipole moment decreases. Also, the coefficient is decreasing function of Lennard-Jones size parameter of oxygen atom. No significant variation of the coefficient was noticed by changing Lennard-Jones energy parameter of oxygen. Finally, authors were able achieve condensation coefficient values of 0.77 and 0.2 (which were reported at more recent experimental studies at that time) by reducing dipole moment of incident molecules to 1.4 D and 0.9 D. As these modifications of dipole moment are unrealistic for water molecules, authors concluded that that these coefficient values of 0.2 and 0.77 at 300 K are unlikely to be correct.

In their work [32], authors used MD simulations in order to study the impact of intramolecular bond flexibility on water cluster formation dynamics by molecular collisions at 300 K temperature. Since the authors were interested in qualitative aspects of flexibility for cluster formations, they used rigid SPC/E water model where the stretching of OH bond was added to the model artificially. They used three different values of OH bond stiffness: $k = 10^3\ kcal/(mol \cdot Å^2)$, $k = 10^5\ kcal/(mol \cdot Å^2)$ and $k = \infty\ kcal/(mol \cdot Å^2)$. The first value of bond stiffness corresponds to the value which is close to commonly used values for flexible molecular models while the $k = \infty$ corresponds to fully rigid case. The second value of stiffness corresponds to hundred times greater stiffness than commonly used value (flexible but very stiff molecule). Authors found that the collision dynamics using stiffer molecules are similar to the rigid case. However, the obtained lifetimes of formed clusters were considerably longer with OH bond stiffness $k = 10^3\ kcal/(mol \cdot Å^2)$. This phenomenon was explained by the stabilization process, which occurs when the part translational energy of colliding

molecules is transfered into vibrational energy. Authors also tried to show that the translational velocity distribution of cluster molecules are Maxwellian and tend to drift lower temperature side during the stabilization process, however, a small system size did not allow authors to obtain conclusive statistics concerning velocity distributions. Overall, obtained results led authors to the conclusion that the higher nucleation rates (which is closely related with evaporation and condensation rates) and higher dimerization probability of two colliding monomers are obtained in molecular dynamics when molecules with realistic values OH stiffness is used since the clusters and liquid phase are more prone to accept the molecules which are colliding to the surface.

1.6. Concluding remarks and formulation of main goal and objectives of the master's thesis

In reviewed scientific literature, there is much research done on phase change boundary conditions at liquid-vapour interphase. The main object of the conducted research is monoatomic or simple polyatomic fluid systems, such argon and water, with few exceptions. However, the research on flexibility effect on these boundary conditions are lacking even though it is property of many polyatomic molecules. The reason for this is that many molecular models (for example in a case of water) were developed to be cost efficient and good at reproducing thermodynamic properties of bulk liquid and there was no need to introduce molecular flexibility to reproduce these properties. Those models later were used in further research on phase change problems for their ability to accurately reproduce bulk liquid properties. However, the evaluation of the molecular flexibility is important for predicting the behaviour of evaporation, condensation and other processes related with molecular collisions, especially, at higher temperatures [33]. The real molecules have more intramolecular degrees of freedom than the rigid molecules, which can be exited, namely the vibrational motion of molecule. Thus, the collision processes simulated by rigid models might not be correct as the realistic molecular collisions are inelastic in terms of the energy of translational and rotational motion. This point can be illustrated by reviewed work [32], in which the authors investigated the dynamics of water cluster formation via molecular collisions using both rigid and flexible models. They showed that additional flexibility has the impact on process dynamics as the lifetime of the cluster increases due to the stabilization effect, which is caused by the energy transfer between translational and vibrational motion.

The main **goal** of the master's thesis is to investigate the effect of molecular flexibility on phase change boundary conditions (such as velocity distributions of evaporation/condensing molecule, condensation/evaporation coefficients etc.) of polyatomic fluids using molecular dynamics simulation method. In this master's thesis, simulations were performed using flexible molecular model of water, which includes harmonic OH bonds and HOH angle vibrations. Water was chosen due to its relatively simple geometric structure and presence of comparable information on the boundary conditions obtained with rigid models. The main **objectives** on master's thesis are:

- investigate the structure of interphase region, determine the thickness of the interphase layer and liquid-vapour boundaries, which are used to investigate phase-change boundary conditions;
- investigate the condensation coefficients from simulation data and compare obtained results with results from scientific literature, where rigid molecular models of water were used;
- investigate energy characteristics of reflected molecules;

- determine velocity distribution functions for evaporation, condensing and reflecting flexible molecules from simulation results and compare the results with analytical relations from scientific literature.

2. Methodology

2.1. Equations of motion

The MD method is based on solving the classical equations of motion for every molecule in the simulation system. Here, word "classical" means that quantum effects in the system are ignored and intramolecular interactions are described by effective potential models, which are obtained from empirical data or from *ab initio* calculations (or combination of these two). The classical equations of motion are sometimes called Newtonian equations of motion and for system of N molecules usually given by

$$m_i \frac{d^2}{dt^2} \boldsymbol{r}_i(t) = \boldsymbol{F}_i, \qquad i = \overline{1;N} \tag{20}$$

where m_i and $\boldsymbol{r}_i$ are the mass and the position vector of the i-th molecule, $\boldsymbol{F}_i$ is the force acting on i-th molecule and t is time.

2.2. Intermolecular interactions

In order to numerically solve the molecular equations of motion, intermolecular forces acting on each molecule must be computed at each timestep. In case of pairwise molecular interactions, the force acting on i-th molecule is the sum of all pairwise interaction forces between all molecular pairs in the system:

$$\boldsymbol{F}_i = \sum_{j=1, j\neq i}^{N} \boldsymbol{F}_{ij}, \qquad i = \overline{1;N} \tag{21}$$

where $\boldsymbol{F}_{ij}$ is the force of pair interaction force between i-th and j-th molecules acting on i-th molecule. Then, if the interaction potential is defined, force $\boldsymbol{F}_{ij}$ can be found from relation:

$$\boldsymbol{F}_{ij} = -\frac{d}{dr} U(r_{ij}) \frac{\boldsymbol{r}_{ij}}{r_{ij}} \tag{22}$$

where $\boldsymbol{r}_{ij} = \boldsymbol{r}_i - \boldsymbol{r}_j$ is the vector connecting the centre of i-th molecule to centre of the j-th molecule and U is the pairwise potential function. In this case, computation of intermolecular interactions requires to compute the distances between all molecular pair in the system, which is very time consuming. To be more exact, the operation number is proportional to squared number of molecules in the system N^2 ($N(N-1)/2$ operations have to be made to find distances between all molecular pairs in the system). Therefore, it might seem that simulation of large systems is impractical and almost impossible. However, there exists algorithms, which provide the possibility to trade some of computational accuracy for the possibility to solve large systems, consisting hundreds of thousands or even millions of molecules.

2.3. Verlet neighbour list and cell list algorithms

In order to reduce computational costs, firstly, one can assume that there is no need to compute interactions between molecules which are far away from each other because they interact weakly and the contribution to total potential energy of the system is low. The distance, at which interaction is still computed, is called cut-off distance r_c. This cut-off distance depends on interaction model and

model parameters used in simulation. However, exclusion of long-distance pairs from energy computations do not reduce computational costs yet because still $N(N-1)/2$ operations have to be done in order to determine which molecular pairs interact and which do not.

One of the methods which allows to reduce computational cost of force calculations is so-called Verlet neighbour list algorithm. The principal scheme of Verlet neighbour list algorithm is given in Fig. 1. In this algorithm, an addition distance r_s is introduced, which is so-called skin thickness. Before computing the intermolecular forces, the lists of molecules within distance of $r_c + r_s$ is made for each molecule. However, computational cost has not yet been reduced because creation of these lists requires number of operations proportional to N^2. The method becomes advantageous in following timesteps when interactions are calculated considering only the molecules included in this list – operation number then becomes proportional to N. The list is updated every few timesteps or when the displacement of at least one molecule in the list becomes larger than r_s. Although updating neighbour lists require order of N^2 operations, lists are not updated every timestep and this this algorithm becomes advantageous when simulations of large systems are performed.

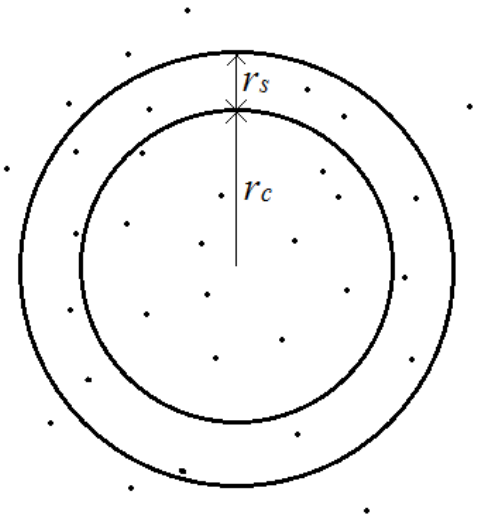

Fig. 6. Principal scheme of Verlet neighbour list algorithm: j-th molecule interacts with particles within the r_c distance. The list contains all molecules within the sphere with radius r_c + r_s. This figure was adopted from [34].

Another simple and widely used algorithm, which helps to reduce computational costs, is cell list algorithm. The main principle of this algorithm in 2D example is shown in Fig. 7. In this algorithm, the simulation domain is divided into cells, which size is equal or greater to the cut-off radius r_c. Then, at each timestep, every molecule is assigned to the cell, in which it is located, and interaction are computed considering molecules, which are located at the same or neighbour cells. For example, j-th molecule in Fig. 7 interacts only with molecules, which are in marked neighbouring cells. Since assignment to the cells require order of N operations, the interaction computation costs are also proportional to N.

Unlike the Verlet neighbour list algorithm, cell list algorithm is difficult to apply for simulations with complex geometries because of the cell division process. On the other hand, difficulty of application of Verlet list algorithm is independent of system geometry. Furthermore, for both methods, the optimal value of r_c must be chosen in large simulations because with large value of r_c, there are many

unnecessary interactions included, which consume computational power. More detailed information about these methods is given in [35–40].

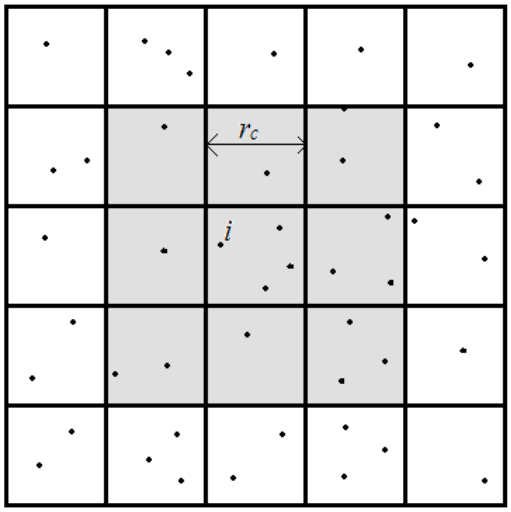

Fig. 7. Principal scheme of cell list algorithm: j-th molecule interacts with particles which are in same or neighbour cells of j-th molecule. This figure was adopted from [34].

2.4. Numerical integration of equation of motion

After the force computations are performed, next important step is to integrate Newtonian equations of motion given by eq. (1). It is clear, that analytical solutions for these equations are too complex to solve analytically even for systems consisting small number of molecules. Therefore, numerical integration tools are used to solve these equations.

There are various numerical integration schemes. However, in order to apply these schemes in any kind of discrete element simulations, they must satisfy the main criteria for given system, which are [41]

- scheme stability in time;
- satisfaction of required accuracy for simulated system;
- conservation of energy and momentum;
- no excess computational memory and costs;
- no additional computation of interaction forces, which is most time-consuming part of dynamics simulations.

One of the widely used numerical integration schemes is Verlet integration algorithm, which is derived from Taylor series of molecular position vector $\boldsymbol{r_i}$ [34]. Formally, the Taylor series of function $f = f(x)$ at pint x_0 is given by:

$$f(x) = f(x_0) + \frac{f^{(1)}(x_0)}{1!}(x - x_0)^1 + \frac{f^{(2)}(x_0)}{2!}(x - x_0)^2 + \frac{f^{(3)}(x_0)}{3!}(x - x_0)^3 + \cdots \tag{23}$$

By adding notations $x = t + \Delta t$, $x_0 = t$ and $\mathbf{O_i}(\Delta t^4) = \frac{r_i^{(4)}\Delta t^4}{4!}$, Taylor series up to the forth member is

$$\boldsymbol{r}_i(t + \Delta t) \approx \boldsymbol{r}_i(t) + \boldsymbol{v}_i(t)\Delta t + \frac{\boldsymbol{a}_i}{2}\Delta t^2 + \frac{\ddot{\boldsymbol{r}}_i}{3!}\Delta t^3 + \mathbf{O_i}(\Delta t^4) \tag{24}$$

where $\boldsymbol{v}_i = d\boldsymbol{r}_i/dt$ and $\boldsymbol{a}_i = d^2\boldsymbol{r}_i/dt^2$ are the velocity and acceleration of *i*-th particle and Δt is the timestep of the numerical integration. Since $\boldsymbol{F}_i = m\boldsymbol{a}_i$, we get that

$$\boldsymbol{r}_i(t + \Delta t) = \boldsymbol{r}_i(t) + \boldsymbol{v}_i(t)\Delta t + \frac{\boldsymbol{F}_i}{2m}\Delta t^2 + \frac{\ddot{\boldsymbol{r}}_i}{3!}\Delta t^3 + \mathbf{O_i}(\Delta t^4) \tag{25}$$

Analogically, it can be shown that

$$\boldsymbol{r}_i(t - \Delta t) \approx \boldsymbol{r}_i(t) - \boldsymbol{v}_i(t)\Delta t + \frac{\boldsymbol{F}_i}{2m}\Delta t^2 - \frac{\ddot{\boldsymbol{r}}_i}{3!}\Delta t^3 + \mathbf{O_i}(\Delta t^4) \tag{26}$$

By adding eq. (25) and eq. (26) we get

$$\boldsymbol{r}_i(t + \Delta t) + \boldsymbol{r}_i(t - \Delta t) = 2\boldsymbol{r}_i(t) + \frac{\boldsymbol{F}_i}{m}\Delta t^2 + 2\mathbf{O_i}(\Delta t^4) \tag{27}$$

Finally, by performing few arithmetical operations it can be show that position of molecule at next timestep is

$$\boldsymbol{r}_i(t + \Delta t) \approx 2\boldsymbol{r}_i(t) - \boldsymbol{r}_i(t - \Delta t) + \frac{\boldsymbol{F}_i}{m}\Delta t^2 \tag{28}$$

New positions of molecules are determined with error of order Δt^4. In Verlet scheme, the velocities of molecules are not used to determine the positions of molecules. However, velocities of molecules can be obtained by subtracting eq. (25) and eq. (26) and performing few arithmetical operations:

$$\boldsymbol{v}_i(t) = \frac{\boldsymbol{r}_i(t + \Delta t) - \boldsymbol{r}_i(t - \Delta t)}{2\Delta t} + \mathbf{O_i}(\Delta t^2) \approx \frac{\boldsymbol{r}_i(t + \Delta t) - \boldsymbol{r}_i(t - \Delta t)}{2\Delta t} \tag{29}$$

Even though positions in the next timestep are determined with error of order Δt^4, the error of Verlet algorithm is of order Δt^2, because it is the error order of velocity determination. Furthermore, the positions of molecules in previous timestep must be saved, which demands a little of additional memory during integration.

By solving system of equations consisted of eq. (28) and eq. (29), molecular positions and velocities can be obtained in every simulation timestep. Even though Verlet algorithm is derived from physical point of view, it can be used to solve any ordinary second order differential equations. From mathematical point of view, it is easy to see the meaning of this method. The numerical solution of the differential equation is obtained by performing "steps" of the function variable (in MD case, variable is time t). At each variable step, the direction of the next step is determined by function

derivatives at the current or/and previous steps. In principle, this means that the less the step of the variable is, the more accurate solutions. However, step cannot be to be infinitesimally small because as value of the step gets smaller, the number of steps required to perform the integration and computational costs increases. Furthermore, with steps that are too small, the errors of arithmetical operations start to add up and accuracy is lost.

The Verlet integration method is widely used method due to its optimal ratio of integration accuracy to computational resources used during integration. However, there are more methods which provide more accuracy or less computational costs. One of the methods, which is simple to implement and is not computationally demanding, is Euler's integration scheme (however, it is not often used method because its accuracy is of order Δt^1). Some of the more accurate but little more demanding Verlet-type methods are leap-frog Verlet, velocity-Verlet, velocity-corrected-Verlet, Beeman and other methods. The more detailed description of these and other more accurate higher order integration methods can be found in [41], [34].

2.5. Molecular models of water

Interaction forces in water and other fluids can be found by performing *ab initio* quantum mechanical computations. This method is highly demanding and only systems containing small number of molecules can be simulated for short periods of time, which are shorter than time periods required to study evaporation/condensation processes. On the other hand, there are effective molecular potential models, which are less demanding. These models are obtained from empirical data and quantum mechanical *ab initio* computations. These effective models for water can be categorized by:

- number of interaction sites in the molecule, which can vary in different molecular models;
- molecular flexibility. Molecular models can be either flexible or rigid. In case of flexible molecules, the bonds and angles are allowed to vibrate and in the case of rigid molecules, lengths of the bonds are kept the same during simulations;
- polarization effects: some models consider polarization effects in the molecule, other ones do not.

2.6. Rigid molecular models of water

Rigid molecular models of water are one of the simplest models used for water simulations. One example of rigid water models is Transferable Intermolecular Potential with 3 Points (TIP3P) model, which has 3 interaction sites located at the centres of oxygen and hydrogens atoms. Since oxygen is more electronegative atom than hydrogen, the charge is distributed in such way that oxygen side of the molecule have negative charge and hydrogen atoms have positive charge – whole molecule becomes electric dipole. Therefore, the negative charge in mostly molecular models, including also TIP3P, is located at oxygen interaction site and positive charge – at hydrogen site. Since the water molecule have neutral charge, the oxygen charge q_O is equal to two times the hydrogen charge q_H. Typically, the sites interact via Coulombic and LJ interactions and the potential energy of interaction of site i with site j is given by

$$U_{intermolecular}(r_{ij}) = 4\varepsilon_{ij}\left[\left(\frac{\sigma_{ij}}{r_{ij}}\right)^{12} - \left(\frac{\sigma_{ij}}{r_{ij}}\right)^{6}\right] + \frac{q_i q_j}{4\pi\varepsilon_0 r_{ij}} \quad (30)$$

where q_i is the charge of i-th site, $r_{ij}$is the distance between i-th and j-th sites, σ_{ij} is the distance at which the LJ potential is equal to zero, ε_{ij} is the depth of the LJ potential well and ε_0 is the vacuum permittivity. The first term in eq. (30) describes the LJ interaction and the second one describes Coulombic interaction. The combination rule to obtain the LJ parameters for unlike interaction sites is the Lorenz-Berthelot (LB) rule:

$$\sigma_{ij} = \frac{\sigma_i + \sigma_j}{2} \quad (31)$$

$$\varepsilon_{ij} = \sqrt{\varepsilon_i \varepsilon_j} \quad (32)$$

Eq. (30) is used to describe many other rigid molecular models of water, which have 3 or more interaction site. For example, in 4-site model case, the negative charge of the oxygen atom is moved to the additional site M, which is placed in the line, which divides HOH angle by half (see Fig. 8). Then, the eq. (30) becomes a bit more complex but still holds: 10 distances must be evaluated in order to calculate the total potential energy of pair of molecules instead of 9 distances, which are required for 3-site model. The model parameters of TIP3P model and few other widely used molecular models of water are given in Table 1. LJ energy parameters for hydrogen sites are not given, because hydrogen sites interact only via Columbic interactions.

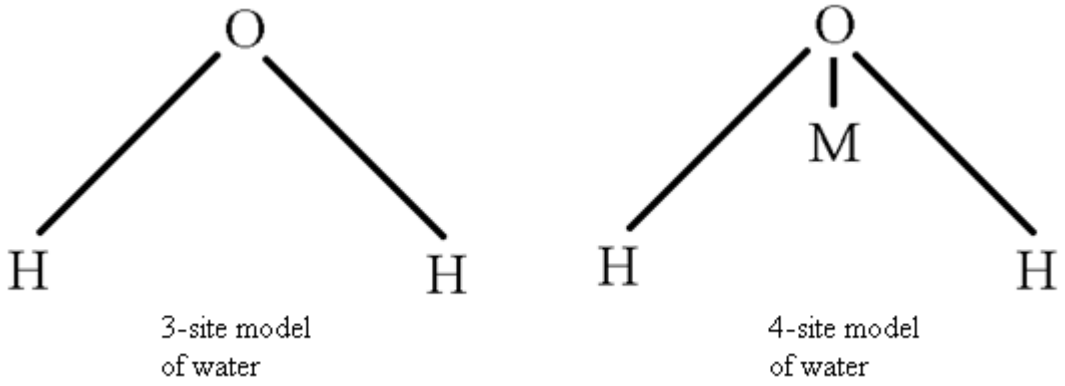

Fig. 8. The geometries of 3 and 4 interaction site models. This figure was adopted from [42].

Table 1. Parameter values of TIP3P, SPCE, BF, TIPS2 and TIP4P water molecular models [43].

	SPC/E	TIP3P	BF	TIPS2	TIP4P
Distance between O and H sites r_{OH}, Å	1	0.9572	0.96	0.9572	0.9572
Angle $\angle HOH$, °	109.47	104.52	105.7	104.52	104.52
LJ distance parameter σ_O, Å	3.1660	3.1507	2.9578	3.2407	3.1536
LJ energy parameter $\varepsilon_O, kJ/mol$	0.65	0.6363	1.3076	0.5418	0.6487
Charge of oxygen site q_O, e	-0.8476	-0.834	0.0	0.0	0.0
Charge of hydrogen site q_H, e	0.4238	0.417	0.49	0.535	0.52
Charge of M site q_M, e	0.0	0.0	-0.98	1.07	-1.04
Distance between O and M sites r_{OM}, Å	0.0	0.0	0.15	0.15	0.15

2.7. Flexible molecular models of water

In standard water molecular models, the water molecule is treated as fully rigid object. These models were developed to reproduce thermodynamic properties of water at ambient temperatures and molecular flexibility was not necessary to achieve that. However, the molecular flexibility of a model becomes important when simulated processes include molecular collisions. The examples of such processes are the formation of the water clusters in vapour and evaporation/condensation of water.

One of the water models which includes flexibility is flexible fixed-point charge (flex-FPC) model, which was developed by [33]. This model was chosen for this work due to its reported ability to reproduce liquid and vapour properties of water in wide temperature range. In this model, the total potential of the system is given as the sum of the intermolecular and the intramolecular potentials:

$$U_{system} = U_{intermolecular} + U_{intramolecular} \tag{33}$$

The term for intermolecular potential is same as in eq. (30). The intramolecular term of the potential consists of harmonic OH bond and HOH angle vibrations as given in by

$$U_{inramolecular} = \frac{1}{2}K_r(r - r_0)^2 + \frac{1}{2}K_\theta(\theta - \theta_0)^2 \tag{34}$$

where K_r is the stiffness of the OH bond, K_θ is the stiffness of the HOH angle vibrations, r_0 is the distance at which the OH bond is at equilibrium, θ_0 is the angle at which the HOH angle is at equilibrium. The parameter values of the model are given in Table 2 and the principal scheme of the model is given in Fig. 9.

Table 2. Flex-FPC molecular model parameter values [33].

r_{OH}, Å	0.9611	$K_r, kJ/(mol \cdot Å^2)$	1480
θ_{HOH}, º	109.4712	$\theta_r, kJ/(mol \cdot rad^2)$	353
q_H, e	0.4238	$\varepsilon_H, kJ/mol$	0.0324
q_O, e	-0.8476	$\varepsilon_O, kJ/mol$	0.6284
σ_O, Å	3.1169	σ_H, Å	0.98

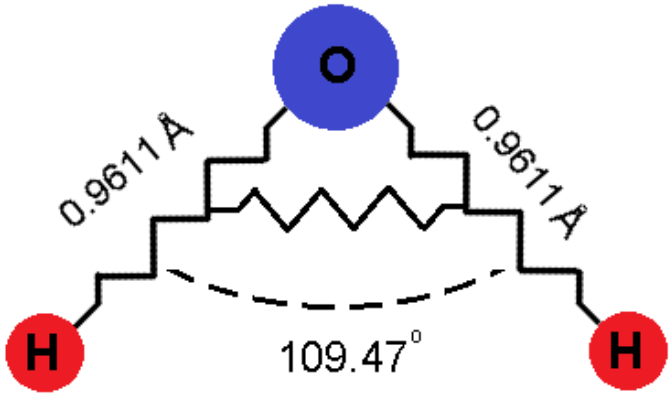

Fig. 9. The principal scheme of Flex-FPC water model. This figure was adopted from [33]

2.8. MD ensembles

Typically, the number of molecules in the system N, the volume of the system V and total energy E_{tot} are constant during simulations. In this case, the simulations are performed in so-called microcanonical ensemble. Microcanonical ensemble is usually noted as (*NVT*) ensemble. Ensemble here means the collective of many different microstates of the system, which correspond to the same macroscopic state. However, sometimes simulations are performed at constant temperatures or pressures. Simulations with constant temperature are carried out in canonical (*NVT*) ensemble and when pressure is also constant, simulations are carried out in isothermal–isobaric (*NPT*) ensemble.

2.9. Definition of simulation temperature

The temperature in the system or subsystem is related with kinetic energy of the molecules and can be expressed as [34]

$$T(t) \equiv \sum_{i=1}^{N} \frac{m_i |\boldsymbol{v}_i(t)|^2}{N_f k_B} \tag{35}$$

where $N_f = 3N - 3$ is the number of degrees of freedom for a system of N molecules with fixed total momentum, $k_B = 1.38 \cdot 10^{-23}\ J/K$ is the Boltzmann constant, m_i is the mass of the i-th molecule and v_i is the velocity of the i-th molecule. The temperature of the process is obtained by averaging the instantaneous temperature over simulation duration. Furthermore, the velocity of molecules can be decomposed into separate terms: translational velocity and rotational velocity (if molecule is flexible, then there is addition term of vibrational velocity). However, the temperature is computed in this master's thesis considering only the translational velocity of molecules and other terms as well as potential energy are considered as internal energy of molecules

2.10. Temperature control during simulations

The temperature in the MD simulations can be controlled by using so-called thermostat methods. There are two main group of thermostats [44]: extended system Lagrangian methods and velocity resampling or rescaling methods. The rescaling methods can keep the average kinetic energy of the system constant but do not necessarily provide correct velocity distributions of (*NVT*) ensemble but are easy to implement with Verlet type integration methods. On the other hand, extended system methods provide true velocity distributions of (*NVT*) ensemble. In both type methods, the intensity of perturbations on time evolution of the system can be regulated by changing thermostat parameters.

An example of second type of thermostat methods is velocity rescaling thermostat. In this method, the molecular velocities are rescaled at each timestep in such way that the temperature of the system would approach the desired temperature T:

$$\boldsymbol{v}_i \to \lambda \boldsymbol{v}_i, \qquad i = \overline{1:N} \tag{36}$$

The rescaling factor λ is typically given by

$$\lambda = \sqrt{\frac{T_0}{T}} \tag{37}$$

where T is the instantaneous temperature of the system or subsystem. However, this method is not suitable to simulate true (*NVT*) ensemble and can only be used when there is need to change temperature of the system rapidly. Berendsen thermostat is similar to velocity scaling method but velocity scaling factor λ here is given by:

$$\lambda^2 = 1 + \frac{\Delta t}{\tau_T}\left[\frac{T_0}{T} - 1\right] \tag{38}$$

An example of extended system methods is Nosé-Hoover thermostat. In this method, the equations of motion of molecules are supplemented by additional constraints, which keeps the kinetic energy constant at desired temperature. The equations of motion in terms of momentum of molecules then is given by [45]

$$\frac{d\boldsymbol{r}_i}{dt} = \frac{\boldsymbol{p}_i}{m_i} \tag{39}$$

and

$$\frac{d\boldsymbol{p}_i}{dt} = \boldsymbol{F}_i - \xi \boldsymbol{p}_i \tag{40}$$

where $\boldsymbol{p}_i = m_i \boldsymbol{v}_i$ is the momentum of i-th molecule. The friction coefficient ξ is given by

$$\frac{d\xi}{dt} = \left(\sum_{i=1}^{N} \frac{\boldsymbol{p}_i^2}{m_i} - N_f k_B T \right) / Q \tag{41}$$

where Q is the parameter, which describes the intensity of temperature control. The friction coefficient ξ is variable quantity, which can have both positive and negative values. If ξ have positive value, the molecules are slowed down and temperature decreases. In opposite case when ξ is negative, the friction accelerates molecules and temperature in the system increases. When instantaneous temperature of the system reached T_0, then ξ approaches to zero. More detailed descriptions of temperature control methods can be found in [44], [45] and [46].

2.11. Simulation descriptions

Simulation methodology of present master's thesis was developed accordingly to methodologies found in scientific papers, where MD simulation studies on liquid-vapour phase change processes were presented. In present master's thesis, there were two simulation series performed:

- liquid-vapour equilibria simulations which were performed investigate the interphase region and test the methodology used in present master's thesis by computing the thermodynamic properties of the water in wide range of temperature from 300 K to 550 K and comparing with results from other works as given in Fig. 10. These simulations were performed using three different water molecular models: TIP3P, SPC/E and flex-FPC.

- liquid-vapour equilibria simulations, which were performed to investigate the phase change boundary conditions in temperature range from 423 K to 503 K as given in Fig. 11. These simulations were performed using only flex-FPC water molecular model.

Simulation system consisted of thin water film placed in the simulation domain, which was prolonged in z direction. Simulations were performed using two rigid TIP3P and SPC/E molecular models and flexible flex-FPC model. In cases of SPC/E and flex-FPC models, additional simulations at 540 K and 550 K were performed to obtain wider temperature range. However, simulations above 500 K for TIP3P model were unsuccessful because the system became violently unstable and it was difficult to determine the transition region between liquid and vapour phases. In each case, the domain geometry used in simulations was rectangular box with prolonged length in z direction and periodic boundary condition applied in all directions. The domain dimensions were approximately 90x93x200 Å. The length of the vapour phase in z axis L_z is chosen to be greater than the mean free path of saturated water vapour molecules in simulated temperature range, which is 148 Å at 420 K temperature [23]. The liquid water film, which consisted of 12000 water molecules, was placed at the centre of the z axis. Initial dimensions of the thin water film were approximately 90x93x45 Å. The detailed information on simulation geometry is given in Table 3.

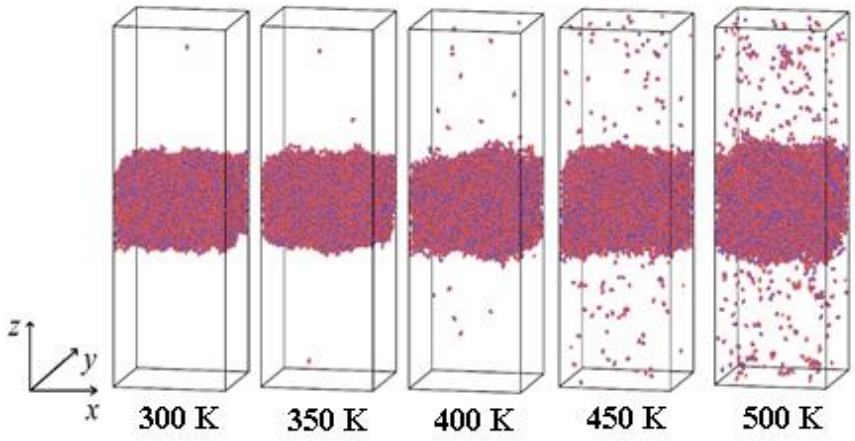

Fig. 10. Snapshots of simulations, which were performed investigate the interphase region and test the methodology used in present master's thesis. These simulations were performed with TIP3P, SPC/E and flex-FPC water molecular models.

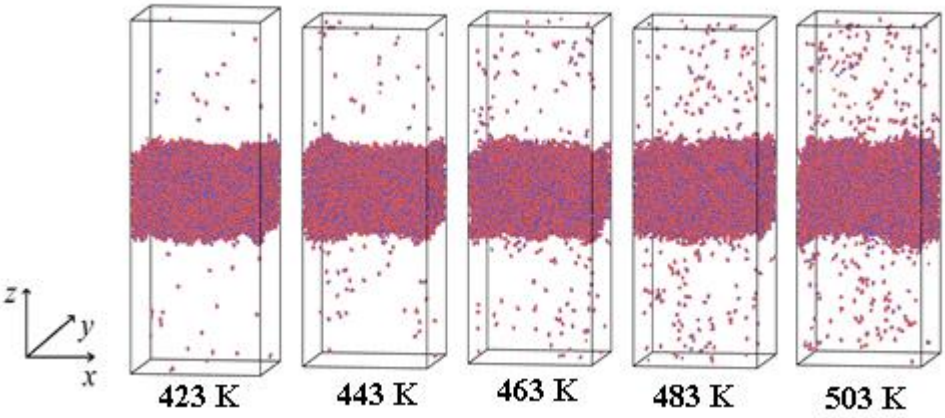

Fig. 11. Snapshots of simulations, which were performed to investigate the phase change boundary conditions. These simulations were performed only with flex-FPC water molecular model.

The initial positions and orientations of molecules were chosen accordingly to FCC crystal lattice. Initial velocities given to molecules were distributed by normal distribution corresponding to the temperature of the simulation, which is defined by eq. (35). The equations of motion (given by eq. (1)) were solved using Verlet integration method with timestep value $\Delta t = 1\ fs$ for SPC\E and TIP3P models and $\Delta t = 0.25\ fs$ for flex-FPC model. The timestep value in simulations with flexible model is lower because period of bond and angle vibrations in the molecules are considerably shorter than time scales of molecular collisions. Therefore, the timestep value has to be lower in order to avoid unphysical increment of total energy in the system and to achieve integration stability. In order to reduce computational resources, Verlet neighbour list algorithm was used with the cut-off distance $r_c = 12$ Å. Long-range interaction summation was done using Particle-Particle Particle-Mesh (PPPM) method.

Table 3. Information about simulation box and water film positions.

Lower and upper boundaries of simulation box and liquid water film in *x*, *y* and *z* axis	Simulation domain	Thin water film
x_{lo}, Å	0.00	0.00
y_{lo}, Å	0.00	0.00
z_{lo}, Å	-80.0	0.00
x_{up}, Å	89.85	44.92
y_{up}, Å	93.37	46.69
z_{up}, Å	125.00	44.01

After the initialization of the system (steps described above), the first equilibration runs were carried out in canonical (*NVT*) ensembles for about 0.1 ns (100000 timesteps for rigid and 400000 for flexible model cases) with temperature control using the Nosé-Hoover thermostat. Temperature control was done every 100 timesteps. After the first equilibration runs, the second equilibration runs were carried out for another 0.1 ns in the microcanonical (*NVE*) ensemble with no temperature control. During this part of simulations, the system reaches liquid-vapour dynamic equilibrium state where the vapour phase is fully saturated, and the evaporation rate is same as the condensation rate. Finally, the sampling runs were performed in the microcanonical (*NVE*) ensemble for about 0.2 ns during which the information of the atoms in the system is sampled for the analysis. The 500 data sets were sampled as sampling was done every 0.4 ps.

In case of simulations, which were used to investigate the boundary conditions, were carried out in a same way as described above with few changes. Firstly, it was noticed that total number of molecules in vapour phase is considerably smaller in lower temperature cases and simulation times required to obtained sufficient amounts of data for analysis were too long. Therefore, simulations were carried out at higher temperatures, namely at 423 K, 443 K, 463 K, 483 K and 503 K temperatures. Secondly, a considerably longer samplings runs were required to gather conclusive statistics of evaporating/condensing molecules: sampling runs were carried out for 4.5 ns (18000000 timesteps). As data was sampled every 0.45 ps, 10000 datasets were obtained during sampling run. Lastly, simulations of such time period are computationally demanding, therefore, these simulations were performed only for flexible flex-FPC water model.

3. Results and discussion

3.1. Cut-off distance selection analysis

The choice of cut-off distance can affect the accuracy of simulation results and computational resources required to carry out these simulations. Typically, cut-off distance for water used in various scientific works vary from 8.5 Å to around 12-14 Å. However, in present master's thesis, the analysis on r_c were performed in order to find optimal value for liquid-vapour phase simulations, which will be carried out for this thesis. Therefore, additional simulations were performed with different values of r_c using SPC/E model. The fitness of r_c on simulations was determined by considering the liquid water density ρ_l at liquid-vapour equilibria. The temperature of this test was chosen to correspond the average temperature of all carried simulations in this master's thesis, which is 400 K. Obtained density results and comparison with experimental and other simulation results of SPC/E model [47] at close temperatures are given in Fig. 12.

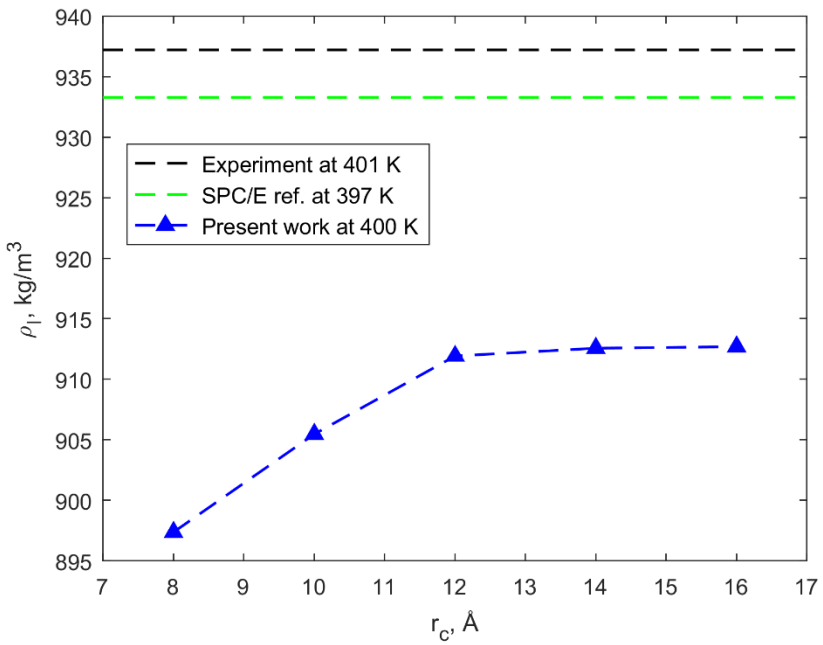

Fig. 12. The dependency of liquid water density on cut-off distance r_c at 400 K. Results obtained from liquid-vapour equilibria state using SPC/E water model. Experimental [48] and SPC/E density values obtained in [47] are given for comparison.

It is seen that with increasing r_c, the liquid density increases as well until r_c reaches 12 Å. With further increment of the r_c, the liquid density asymptotically approaches the constant value of liquid density of SPC/E model at given temperature. The further increasement of r_c after this point further increases computational costs, however, the increasement of accuracy is negligible. Therefore, it was chosen to perform simulations with $r_c = 12$ Å. Furthermore, it can be seen that the liquid density approaches the value which is considerably lower than the value obtained in [47] at 397 K and even more distant that the experimental density at 401 K. The reason for this is that the developed water models are not

able to accurately predict all experimental water properties in wide range of temperature and there are noticeable deviations. On the other hand, the deviation from luqid density obtained by same molecular model at same temperature in [47] may be explained by difference in simulation parameters, which were used in present master's thesis.

3.2. Investigation of interphase region

The aim of this part of research was to investigate the structure of interphase region and determine the thickness of the interphase layer and also to test the simulation methodology used in present master's thesis. Therefore, simulations of water liquid-vapour equilibria in temperature range from 300 K to 500 K were performed with two rigid water models TIP3P and SPC/E and one flexible water model flex-FPC. The methodology will be tested by comparing vapour and liquid densities obtained with these models with the results obtained in other works. Therefore, it is necessary to determine individual regions in the simulation domain, namely, the liquid phase, vapour phase and interphase. Such information can be obtained from density profiles of the simulated system along z axis. The density profiles obtained by flex-FPC model at 300 K, 350 K, 400 K and 450 K are given in Fig. 13.

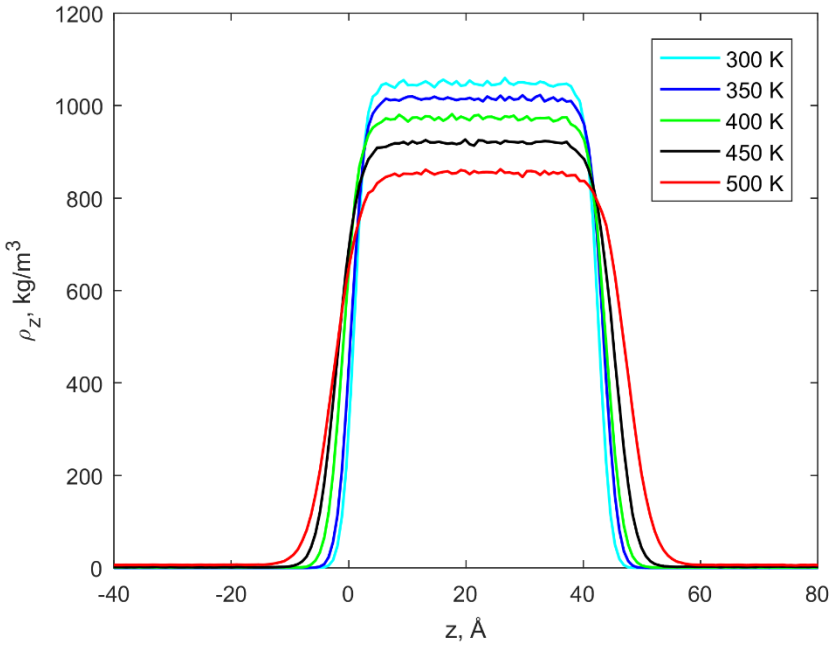

Fig. 13. Density profiles of the system obtained by flex-FPC model at four different temperatures.

These density profiles for each temperature were computed by dividing the simulation box into layers (the layer thickness is $\Delta z = 0.75$ Å) and summing the mass of molecules, which are located within the layer at given time. Then, the density of each layer was obtained by dividing the mass of molecules by the volume of the layer. This way, a total of 500 temperature profiles were obtained in each simulation, which corresponds to 500 sampled datasets. The final result is obtained by averaging over these 500 datasets. The averaging procedure was done in order to reduce the effect of density

fluctuations in the system, which occur due to a finite size of the simulated system. From given figure, it can be seen that there are three distinct regions in the system: the vapour phase region with the density of saturated vapour; the liquid phase region with the density of bulk liquid and the interphase region, where the density continuously decreases form the liquid phase density to the vapour phase density. Furthermore, it can be seen that liquid density decreases and the thickness of interphase region increases with increasing simulation temperature.

As suggested in [23], the interphase region density can be accurately approximated using hyperbolic tangent function:

$$\rho(z) = \frac{1}{2}(\rho_v + \rho_l) + \frac{1}{2}(\rho_v - \rho_l)\tanh\left(\frac{z - z_0}{\delta}\right) \tag{42}$$

where ρ_l is the liquid phase density, ρ_v is the vapour phase density, z_0 is the middle point of the interphase and δ is the meassure of the interphase thickness. The example of interphase density profile obtained with flex-FPC model at 400 K is given in Fig. 14. Similar results as described above were obtained for both TIP3P and SPC/E models.

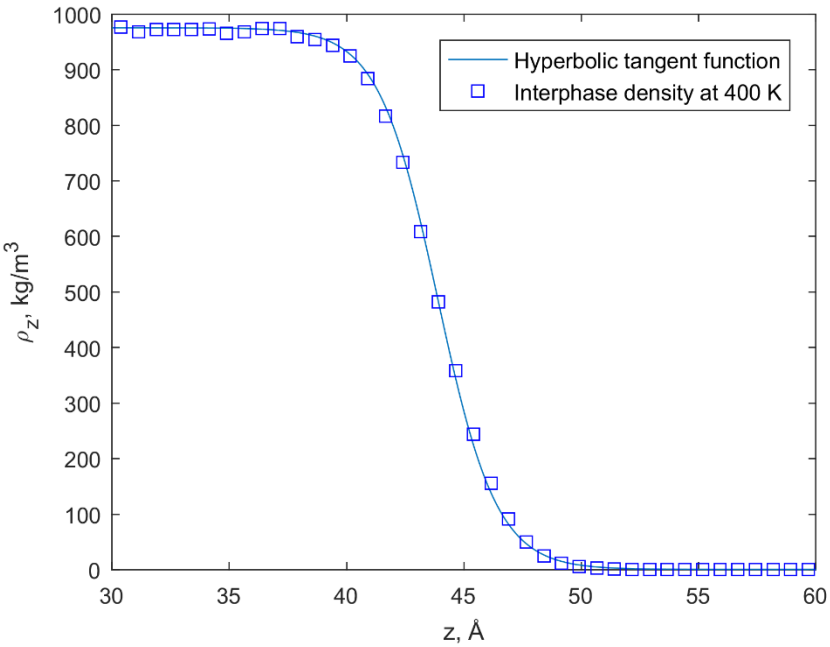

Fig. 14. The interphase density profile obtained with flex-FPC model at 400 K. Filled squares represent modelling results and the dotted line represent the fitting function given by the eq. (42).

The "10-90" thickness of the interphase or the interphase thickness d_{10-90}, which is a distance over which the density at the interphase drops from 90 % of liquid density to 10 % of liquid density, is related to the measure of interphase thickness by relation $d_{10-90} = 2.1972\delta$. Interphase thickness values obtained in simulations are given in Table 4. The value of d_{10-90} increases with increasing temperatures and varies from 4.62 Å to 12.14 Å in temperature range from 300 K to 500 K for TIP3P model. In case of SPC/E model, d_{10-90} varies from 4.35 Å to 15.75 Å in slightly wider temperature range from 300 K to 540 K. Finally, d_{10-90} varies from 4.36 Å to 11.71 Å in temperature range from 300 K to 550 K for flex-FPC model. As mention before, simulations above 500 K point with TIP3P

model were unsuccessful because of the difficulties of determining the transition between liquid and vapour. Same problem occurred above 540 K temperature for SPC/E model and above 550 K for flex-FPC model. Therefore, some of the values in the table are missing.

Table 4. Values of interphase thickness obtained in simulations at various temperatures with TIP3P, SPC/E and flex-FPC molecular models.

	10-90 thickness of the interphase d_{10-90}, Å		
Temperature T, K	**TIP3P**	**SPC/E**	**Flex-FPC**
300	4.62	4.35	4.36
350	5.99	5.45	4.99
400	7.27	6.38	5.53
450	9.75	7.85	7.20
500	12.14	10.32	8.30
540	-	15.75	-
550	-	-	11.71

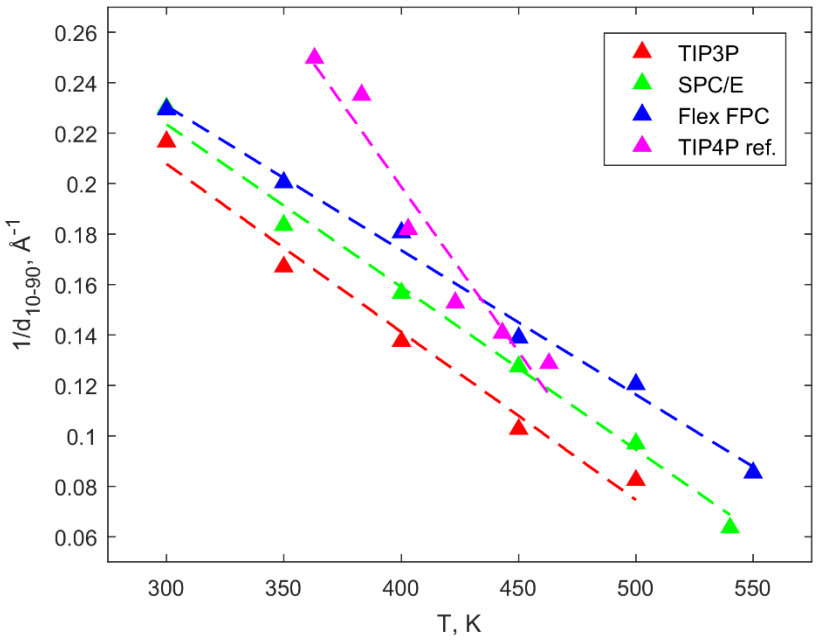

Fig. 15. The interphase thickness as a function of temperature. TIP4P model data for comparison is taken from [15].

One over interphase thickness $1/d_{10-90}$ values and comparison with TIP4P model results from [15] are given in Fig. 15. It can be seen, that the $1/d_{10-90}$ is a decreasing linear function of temperature and can be approximated by

$$1/d_{10-90} = A + BT \qquad (43)$$

where A and B are function coefficients obtained by regression. The coefficient values for eq. (43) are given in Table 5.The results obtained by different models in present master's thesis are close to each other and decreases almost at the same rate. On the other hand, the $1/d_{10-90}$ decreases more rapidly in the case of TIP4P model. This difference in $1/d_{10-90}$ behaviour can be explained by the geometrical differences of the molecular models, which were used in present master's thesis and work [15]. The TIP4P model has four interaction sites, which means that the oxygen charge location is displaced to the point M as shown in Fig. 8. This may lead to a different system behaviour at same conditions and, therefore, the some of the system properties may differ from 3-site models.

Table 5. Coefficient values for 1/d"$_{10\text{-}90}$" function given by eq. (43) with additional information on temperature intervals in which these coefficients hold and values of R^2.

Model	Temperature interval ΔT, K	Parameter A, Å^{-1}	Parameter B, K^{-1}Å^{-1}	R^2
TIP3P	300-500	-0.0006658	0.4075	0.98
SPC/E	300-540	-0.0006448	0.4169	0.99
Flex-FPC	300-550	-0.0005724	0.4025	0.99
TIP4P [15]	363-483	-0.00131	0.7227	0.94

3.3. Liquid and vapour densities at liquid-vapour phase equilibria

The comparison of liquid and vapour phase densities with experimental values and the results obtained by other authors are given in Fig. 16. It is seen from the figure that the computed densities for liquid phase deviate the most from the experimental values for TIP3P model and this deviation increases with increasing temperature. It is worth mentioning that the number of evaporation events was low and there were only few molecules in vapour phase in simulations bellow 400 K temperature. Therefore, vapour densities obtained in present master's thesis might be inconclusive in temperatures below 400 K even though they visually seem to be close to the experiment at those temperatures in representation.

a) b)

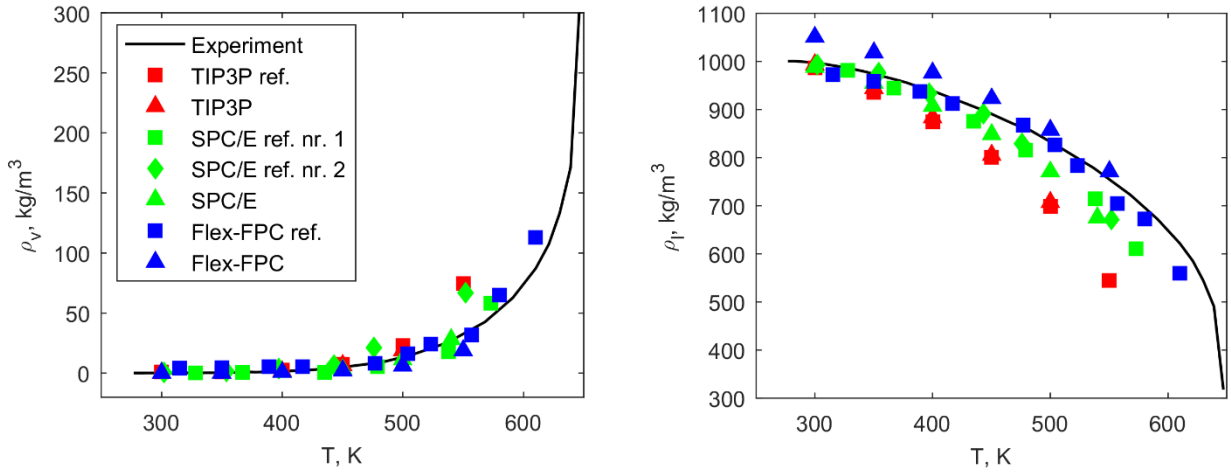

Fig. 16. The density as a function of temperature in liquid-vapour phase equilibria for: a) liquid phase; b) vapour phase. The experimental values is taken from [48], data for TIP3P ref. is taken from [49], data for SPC/E refs. nr. 1 and nr. 2 is taken from [50] and [47] and data for Flex-FPC ref. is taken from [33].

From Fig. 16 b), it can be seen that the deviation of liquid density from the experimental values changes at different temperatures. To characterise this change, the relative deviation of liquid density from the experiment is defined as

$$s(T) = \frac{\rho_{l,exp}(T) - \rho_l(T)}{\rho_{l,exp}(T)} \cdot 100\ \% \tag{44}$$

where $\rho_{l,exp}$ is experimental liquid density at liquid-vapour phase equilibria and ρ_l is liquid density obtained from simulations. It is worth noticing that the numerator in eq. (44) is not an absolute value of the difference and, therefore, value of s can be both positive and negative. When simulated density is lower than experimental density, s value is positive and in opposite case, the value of s is negative. The s values at different temperatures are given in Fig. 17. The deviations of TIP3P model results obtained in present master's thesis are in good agreement with the ones obtained in [49]. The deviations of SPC/E also are in a good agreement with results of [50] but slightly differs from [47]. These slight differences can be explained by systematic errors which occur in simulations due to different simulation geometries, numerical integration methods, timestep values and other simulation parameters. However, the differences of s are significantly greater in case of Flex-FPC model. The value of s for the results from [33] is close to 0 % in almost whole temperature range and exceeds 5 % value only when temperature is above 550 K. On the other hand, s value for Flex-FPC model results in present master's thesis is negative in whole temperature range from 300 K to 550 K. The additional sensitivity analysis of simulation parameters (such as timestep value, cut-off distance and etc.) were performed by carrying out simulations with different parameter values. However, the results from [33] could not be reproduced. The explanation for this significant difference may be the effect of finite size of the system and different computation methods: authors used NVT-Gibbs ensemble Monte Carlo (GEMC) technique and the coupled-decoupled configurational-bias Monte Carlo (CBMC) algorithm with 350-450 molecules for the phase equilibrium simulations. As MD technique used in present master's thesis can reproduce the density results of TIP3P and SPC/E models, it can be concluded that techniques used in [33] may not be correct for liquid-vapour phase equilibria simulations. Furthermore, since the aim of present master's thesis was to investigate the effect of molecular flexibility on water phase change boundary conditions, the flex-FPC model suitable and will be still used in further investigation.

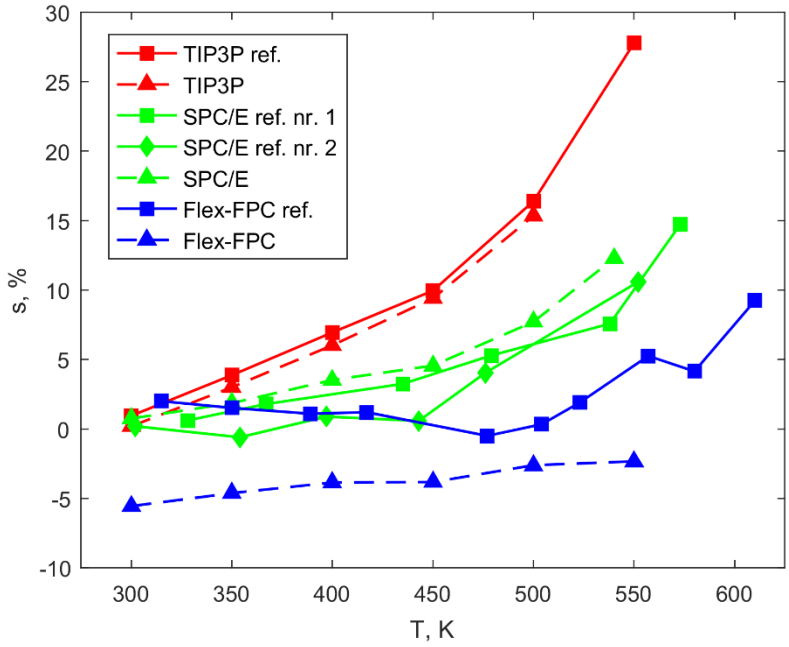

Fig. 17. The relative simulated density deviation from experimental results (defined by eq. (25) as function of temperature. The experimental values is taken from [48], data for TIP3P ref. is taken from [49], data for SPC/E refs. nr. 1 and nr. 2 is taken from [50] and [47] and data for Flex-FPC ref. is taken from [33].

3.4. Counting of evaporation/condensation/reflection events at the interphase

In this section, the liquid-vapour phase change boundary conditions will be investigated using only flex-FPC water model in temperature range from 423 K to 503 K. In present master's thesis, evaporation evens at the interphase were counted using two boundaries as described in work [25]. One of the boundaries is placed in vapour phase and other one is placed in liquid phase as given in Fig. 18. Evaporation event was registered when liquid molecule crosses vapour boundary after crossing the liquid boundary. Reflection was registered when vapour molecule enters the region between boundaries by crossing vapour boundary and then leaves it by crossing vapour boundary second time from the other side. Finally, the condensation event was registered when vapour molecule crosses vapour boundary and then enters liquid phase by crossing liquid boundary. To determine positions of these boundaries, new coordinate in z axis was defined

$$z^* = \frac{z - z_0}{d_{10-90}} \tag{45}$$

where z_0 is the middle point of the interphase (see eq. (42)). The recommendation for liquid boundary position given in [25] is in range of $2 \leq z^* \leq 4$. In present master's thesis, the vapour boundary was placed at $z^* = 2$. The position of liquid boundary was the same as in [25]: $z^* = -1$.

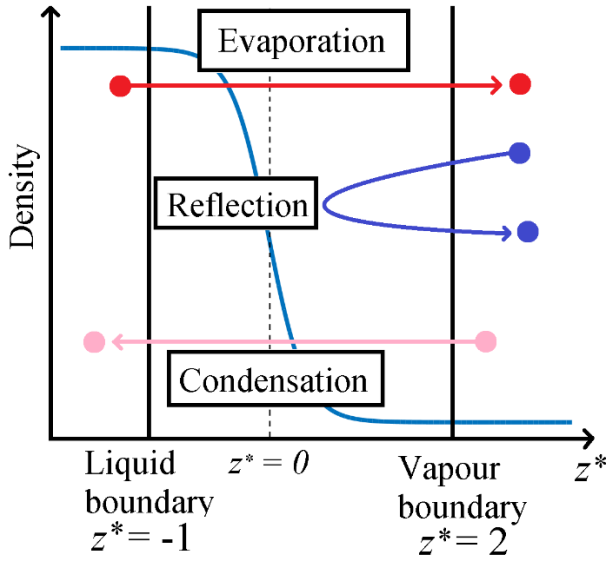

Fig. 18. Schematic representation of method used to calculate evaporation, condensation and reflection events. This figure was adopted from [25].

At the beginning of sampling part of evaporation simulations, part of molecules in the system is placed between liquid and vapour boundaries. These molecules distort the results of evaporation/condensation processes because they cross the boundaries, but events are not registered (because these molecules cross only one boundary when they leave the region between the boundaries). Therefore, it is important to determine the influence of these molecules on the results. The evolution of number of molecules initially placed between boundaries at 423 K case is given in Fig. 19. The evolution is given for 423 K case because it is the lowest temperature of evaporation/condensation simulations carried with Flex-FPC model. In higher temperature cases, molecules placed between the boundaries exit this region faster due to more intense diffusion into bulk liquid and higher evaporation rates into vapour phase. From this figure, it can be seen that the number of molecules initially placed between the boundaries approaches zero before 0.1 ns mark, which makes only 2.22 % of total simulation time. Therefore, it is assumed that these molecules have no influence on the results and their effect is neglected.

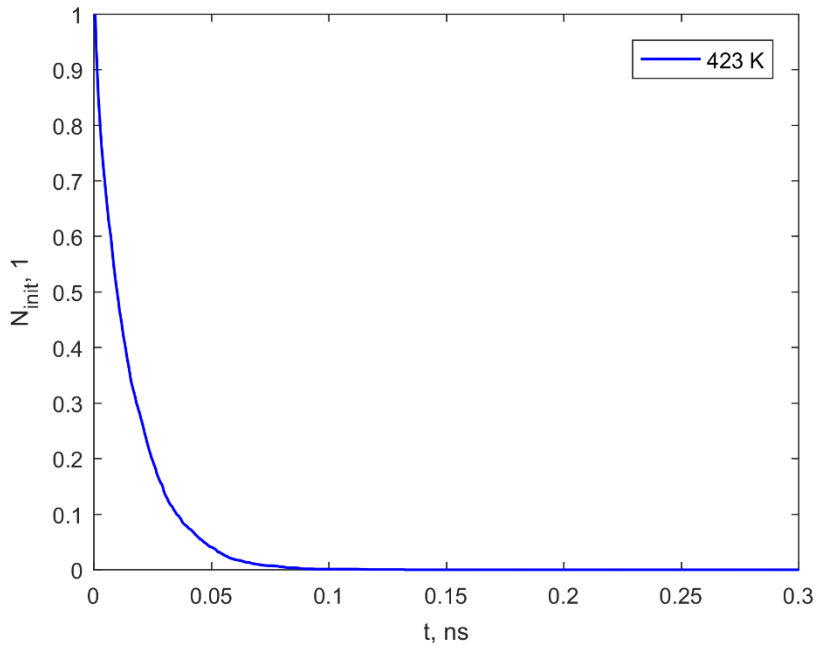

Fig. 19. Time evolution of number of molecules, which were placed between liquid and vapour boundaries at beginning of the simulation at 423 K temperature.

3.5. Condensation coefficients

If molecular exchange phenomena is not considered, the condensation coefficient is defined as the ratio of number of condensed molecules to the number of all molecules that impinge on the surface:

$$\sigma_c(\xi) = \frac{N_c(\xi)}{N_{all}(\xi)} = \frac{N_c(\xi)}{N_c(\xi) + N_r(\xi)} \tag{46}$$

where N_c is the number of condensed molecules, N_{all} is the number of all vapour molecules which impinged on the interphase, N_r is the number of molecules which impinged on the interphase from the liquid phase but was reflected back to the vapour phase and ξ is any property of impinging molecules. In present master's thesis, ξ is the surface-normal and surface-tangential components of translational motion energy E_z, E_x and E_y and energy of rotational motion E_{rot}. The obtained results using flex-FPC water model are given in Fig. 20, where the condensation coefficient is given as the function of E_z. Here, the energy of motion here is expressed in units of K. Simulation results in 423 K was excluded because there were not enough condensation and reflection events during the simulation to gather sufficient statistics. It can be seen that the condensation coefficient decreases when the liquid temperature rises and increases with increasing value of E_z. The molecules with higher values of E_z can penetrate into deeper layers of the interphase during the impact and the chance of making hydrogen bonds with interphase molecules. Therefore, the likelihood of condensation increases. Also, more energetic interphase molecules reflect the impinging molecules more easily. Furthermore, coefficient values obtained in present master's thesis is considerably higher than the values obtained in [17], where rigid SPC/E molecular model of water was used. This difference can be explained by stabilization effect occurring when the part of translational motion energy is transferred to vibrational energy of two or more colliding flexible molecules as suggested in [32]. Therefore, reflection

likelihood of flexible molecule is lower. Furthermore, the obtained results in this master's thesis can be well approximated by analytical function as in [17]:

$$\sigma_c = \alpha \left[1 - \beta \exp\left(-\frac{E_z}{k_B T}\right)\right] \tag{47}$$

where α and β are function parameters, which are found by regression analysis. Values of α and β and average condensation coefficients are given in Table 6.

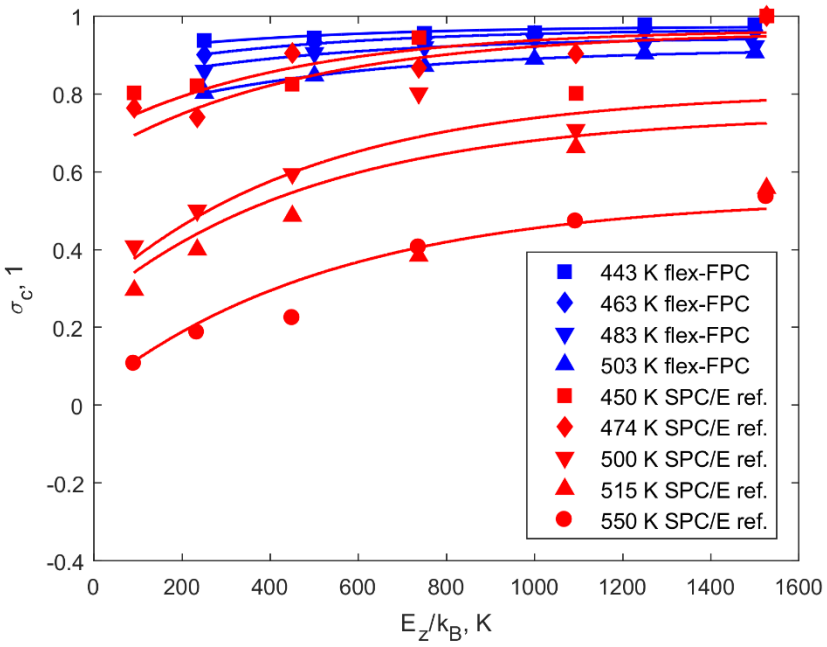

Fig. 20. Condensation coefficient of water as a function of surface-normal component of translational energy of impinging molecules. Condensation coefficients obtained with rigid SPC/E water model in [17] is given for comparison.

Table 6. Condensation coefficient parameter values for eq. (9) and average values of condensation coefficient.

Temperature T, K	α	β	$\bar{\sigma}$
443	0.9740	0.07686	0.9581
463	0.9672	0.1165	0.9420
483	0.9462	0.1346	0.9128
503	0.9163	0.2053	0.8701

The dependencies of condensation coefficient on surface-tangential components of translational energy and total rotational energy are given in Fig. 21 and Fig. 22. It can be seen that value of σ_c is independent of $E_{x,y}$ and is constant below $E_{x,y}/k_B = 800$ point. Above this point, the value of σ_c

starts to scatter and no tendency of σ_c could not be determined. The reason for the scattering of data might be an insufficient statistic because the number of impinging molecules with higher energies is significantly lower than number of molecules impinging with lower energies. In case of rotational motion energy, the values of σ_c is also independent of E_{rot}.

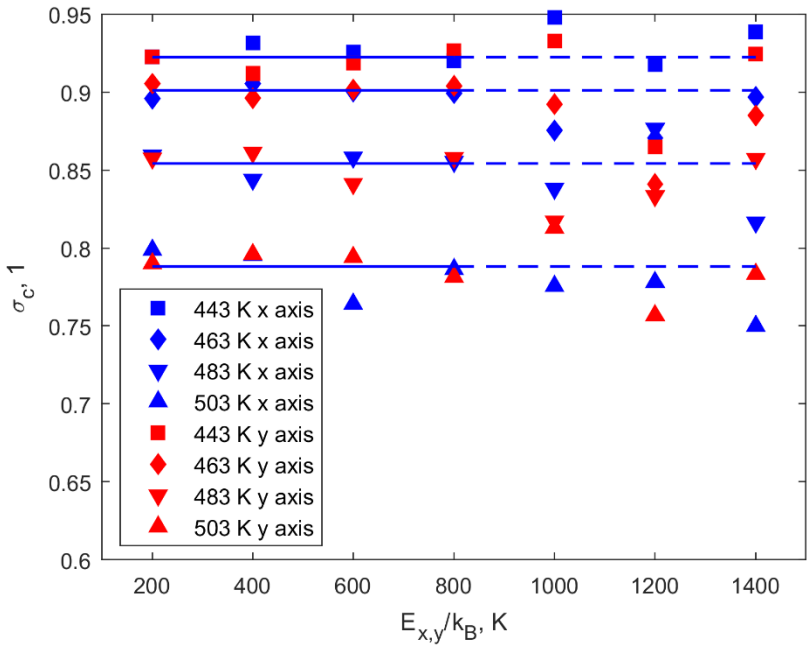

Fig. 21. Condensation coefficient of water as a function of surface-tangential components of translational energy of impinging molecules.

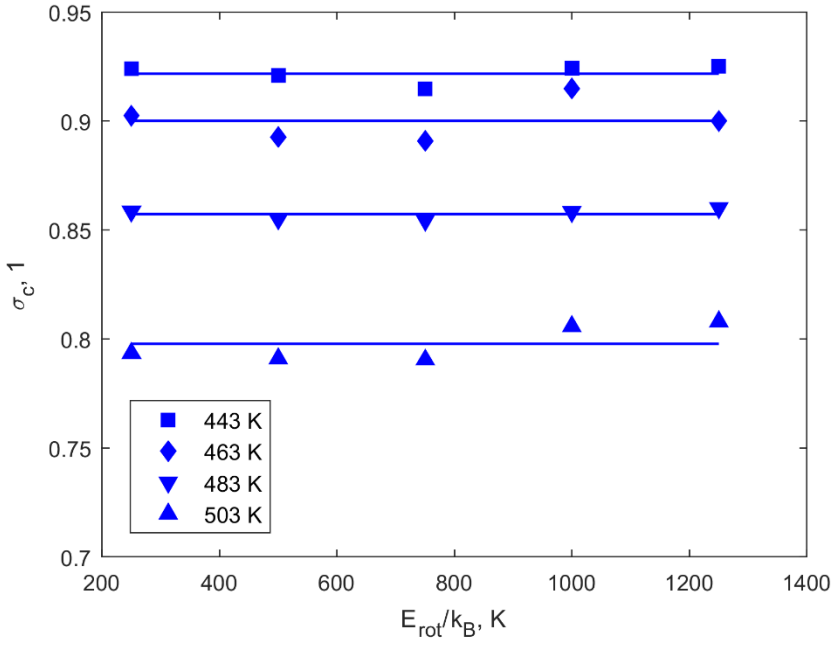

Fig. 22. Condensation coefficient of water as a function of energy of rotational motion of impinging molecules.

3.6. Energy change of reflecting molecules

As seen above, the considerable amount of vapour molecules, which impinge on the interphase, is reflected back to the vapour phase. The information about energy characteristics of these molecules is also important for phase change boundary conditions. Energy changes of surface-normal and surface-tangential components of translational motion of reflected molecules are given in Fig. 23 and Fig. 24. The energy change during reflection is defined as the difference between energy of molecule after the reflection and energy of molecule before the reflection:

$$\Delta E_i = E_i^{After\ reflection} - E_i^{Before\ reflection} \tag{48}$$

Here, the energy of impinging molecules, i.e. the energy before reflection $E_i^{Before\ reflection}$ is denoted as simply as E_i, where i denotes component or type of energy ($i = x, y, z, rot$). From these figures, it can be seen that the part of molecules, which have small energy components in x, y and z directions before reflection, undergo an increase in energy of respective components during the reflection process. On the other hand, the molecules with high translational energy components in x, y and z directions loses part of the energy of respective component.

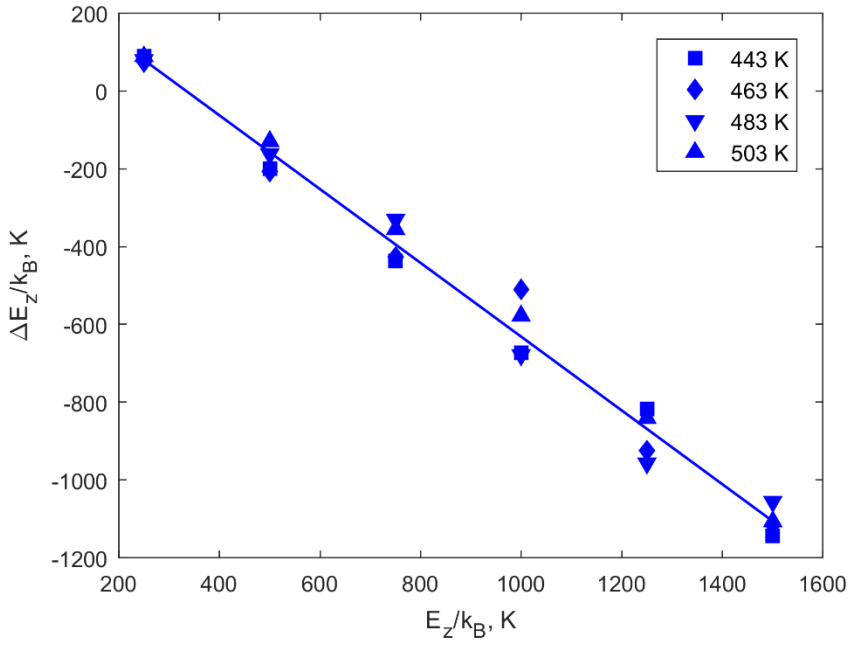

Fig. 23. Energy changes of surface-normal component of translational motion of reflected molecules.

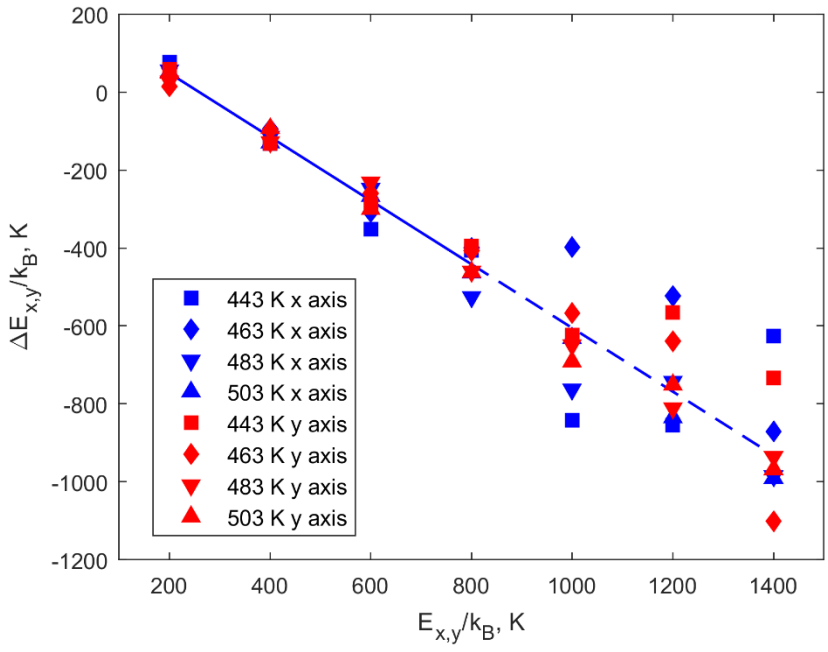

Fig. 24. Energy changes of surface-tangential components of translational motion of reflected molecules.

Similar tendency can be seen for the rotational energy of reflecting molecules (see Fig. 25). In this case, the $\Delta E_{rot} = 0$ point is shifted to the higher values of E_{rot}, which means that the molecules reflect with higher energies up to the point of impinging molecule energy $E_{rot}/k_B \approx 700$ K. Molecules with higher rotational lose part of their rotational energy during reflection. The gains and losses of x, y and z components of translational energy and rotational energy might not be only the result of thermal interaction of reflecting molecules with the interphase but also it might be the result of energy transfer between these components of energy. Furthermore, for all cases, the change in energy is a linear function of the energy of impinging molecules and can be approximated by

$$\Delta E_i = A + BE_i \tag{49}$$

where ΔE_i is the change in energy ($i = x, y, z, rot$), E_i is the energy of impinging molecule and A and B are constants found by regression. Values of A and B for each case is given in Table 7. It is worth mentioning that in the case of $E_{x,y}$ (see Fig. 24), linear function approximates simulation results only bellow the point $E_{x,y}/k_B = 800$ K. Above this point values of $\Delta E_{x,y}$ start to scatter and no trend of $\Delta E_{x,y}$ was found.

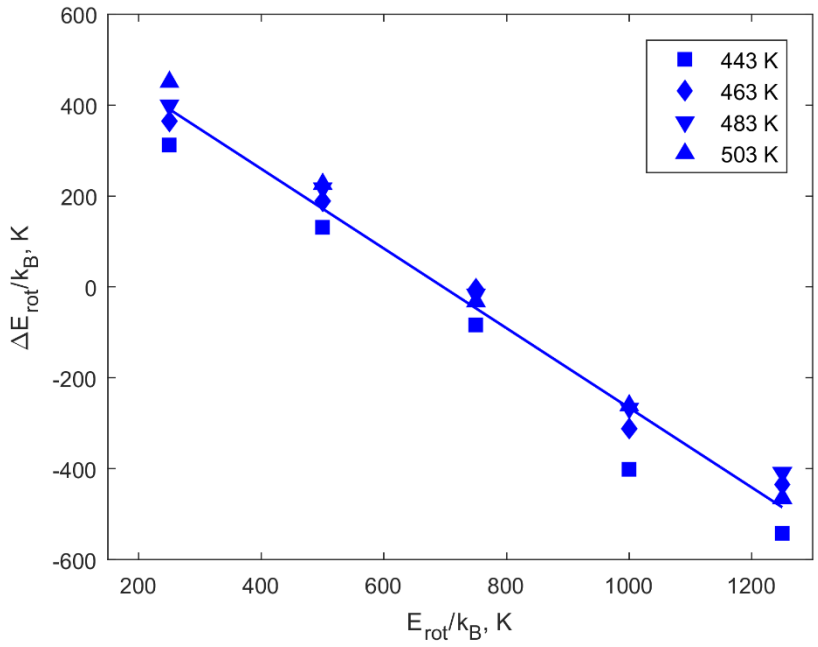

Fig. 25. Energy changes of rotational motion of reflected molecules.

Table 7. Parameter values for eq. (49).

	$A \cdot 10^{-21}$, J	B, 1	R^2
Energy of surface-normal component of translational motion E_z	4.363	0.9478	0.9866
Energy of surface-normal component of translational motion $E_{x,y}$	2.922	0.8169	0.9726
Energy of rotational motion E_{rot}	8.419	0.8755	0.9725

3.7. Velocity distribution functions evaporating and condensing molecules

The velocity distribution functions of evaporating, condensing and reflecting molecules were investigated for 503 K simulation case. The sampling numbers of evaporated, condensed and reflected molecules are given in Table 8. As seen from the table, the number of evaporation events is almost the same as number of condensation events. However, the number of reflection events are considerably smaller. The distribution functions obtained from the simulation for surface-tangential and surface-normal components of translational velocity v_x, v_y and v_z are given in Fig. 26, Fig. 27 and Fig. 28. From these figures, it can be seen that the velocity distribution functions in x and y axis obtained in simulations ideally agree with the Maxwellian distribution given by

$$F_{x,y}(v_{x,y}) = \left(\frac{m}{2\pi k_B T}\right)^{\frac{1}{2}} \exp\left(-\frac{m v_{x,y}^2}{2k_B T}\right) \tag{50}$$

where m is the mass of the molecule, T is the liquid temperature and v is velocity of the molecule. On the other hand, the mean velocity of evaporating and condensing molecules in z axis is slightly higher than the mean velocity of Maxwellian distribution at liquid temperature, which is given by

$$F_z(v_z) = \left(\frac{m}{k_B T}\right) v_z \exp\left(-\frac{m v_z^2}{2k_B T}\right) \tag{51}$$

Authors in [16] suggested a modification of Maxwellian distribution given by eq. (52) to give better explanation for evaporating and condensing molecules in simulations. This modification includes the condensation coefficients obtained from eq. (47) and is given by

$$F_{z,e}(v_z) = \frac{1 - \beta \exp(-m v_z^2/(2k_B T))}{1 - \beta/2} \left(\frac{m}{k_B T}\right) v_z \exp\left(-\frac{m v_z^2}{2k_B T}\right) \tag{52}$$

Here, the velocity distribution of evaporating and condensing molecules is modified by σ_c. It is worth mentioning, that v_z values of condensing molecules are negative and, therefore, the absolute value of v_z was used to compute the probability distribution functions.

Table 8. Number of events sampled during 503 K simulation.

	Number of events
Evaporation	25285
Condensation	25286
Reflection	6469

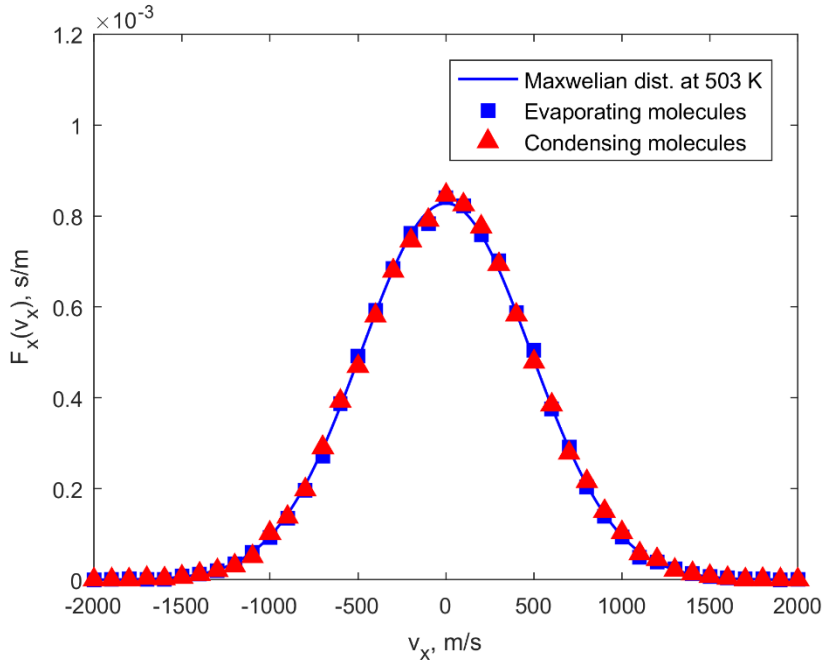

Fig. 26. Velocity distribution function of evaporating and condensing molecules in *x* direction.

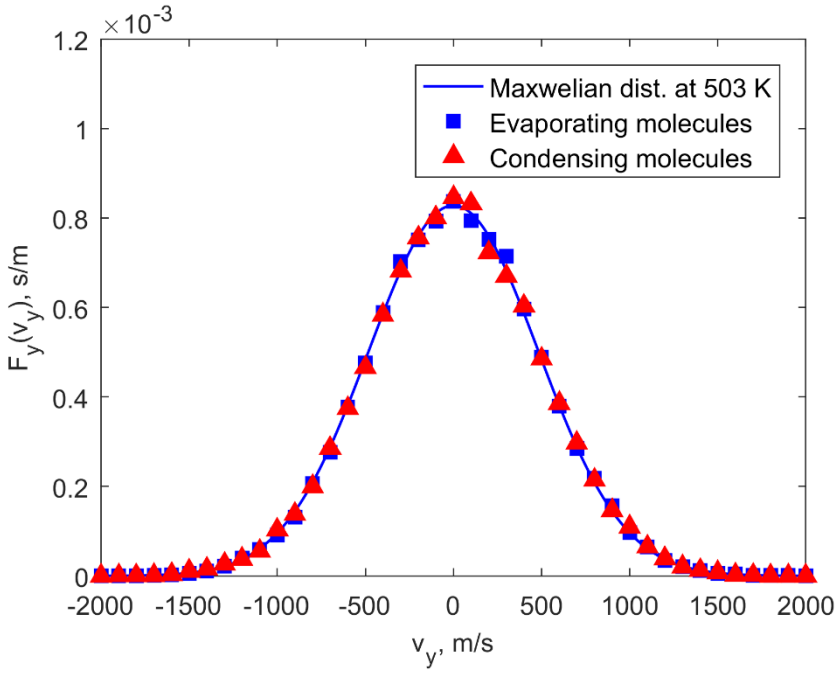

Fig. 27. Velocity distribution function of evaporating and condensing molecules in *y* direction.

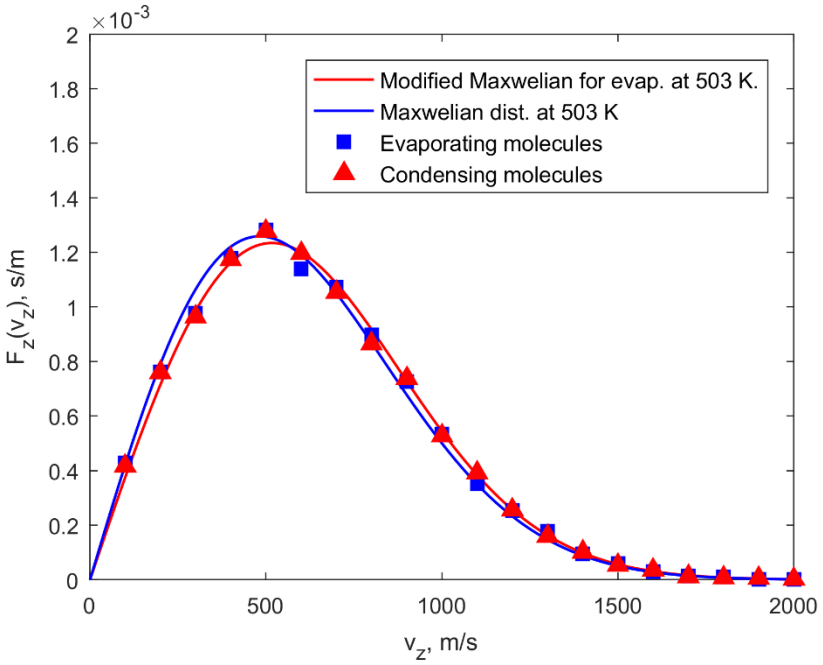

Fig. 28. Velocity distribution function of evaporating and condensing molecules in *z* direction.

3.8. Velocity distribution function reflecting molecules

The distribution functions of v_x, v_y and v_z for reflecting molecules and molecules before reflection are given in Fig. 29, Fig. 30. It can be seen that the probability density functions of v_x and v_z for reflecting molecules are well described by eq. (50) in velocity intervals $v_{x,y} \epsilon [-\infty ; -400]\ m/s$ and $v_{x,y} \epsilon [400; +\infty]\ m/s$. However, in interval $v_{x,y} \epsilon [-400; 400]\ m/s$, the probability density function starts to scatter and the values of the function tend to be lower than the theoretical distribution, with few exceptions. In both reflection and before reflection cases, the maximum values of distribution function at point $v_{x,y} = 0\ m/s$ is lower than the theoretical prediction. This scattering might be the result of insufficient statistical data obtained for reflecting molecules.

In case of velocities in surface-normal direction (see Fig. 31), the value of probability density function is higher than the Maxwellian distribution in lower velocity region and is lower in higher velocity region, i.e. the mean value of v_z is significantly lower and the velocity distribution function is shifted to the lower velocity side. Interestingly enough, the velocity distribution function of molecules before reflection is almost the same and is also shifted to the lower velocity side. Similar results for reflecting argon molecules were obtained in [16] and [25], however, authors did not explain the reason for this phenomena. Furthermore, the modification of Maxwellian distribution for reflecting molecules was also suggested in [16] and is given by

$$F_{z,r}(v_z) = \frac{1 - \alpha + \alpha\beta \exp(-mv_z^2/(2k_BT))}{1 - \alpha + \alpha\beta/2} \left(\frac{m}{k_BT}\right) v_z \exp\left(-\frac{mv_z^2}{2k_BT}\right) \qquad (53)$$

This time, the velocity distribution of reflecting molecules is modified by $(1 - \sigma_c)$. It is seen that eq. (53) well describes the v_z distribution in interval $v_z \epsilon [800; +\infty]\ m/s$. However, the significant

deviation still exists in velocity interval $v_z \in [0; 800]\, m/s$ and the distribution function for reflecting molecules reaches its maximum value at lower value of v_z when compared to eq. (53).

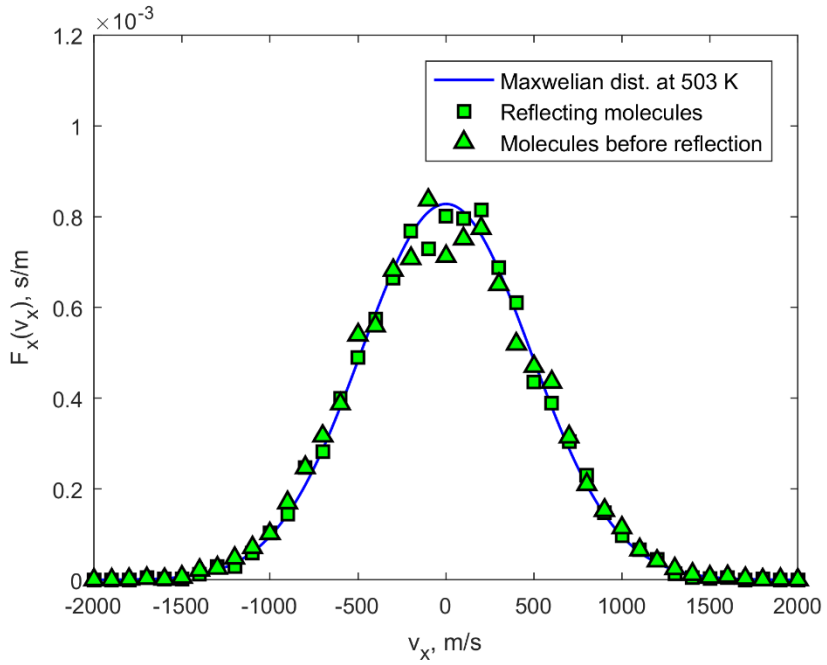

Fig. 29. Velocity distribution function of reflecting molecules in *x* direction.

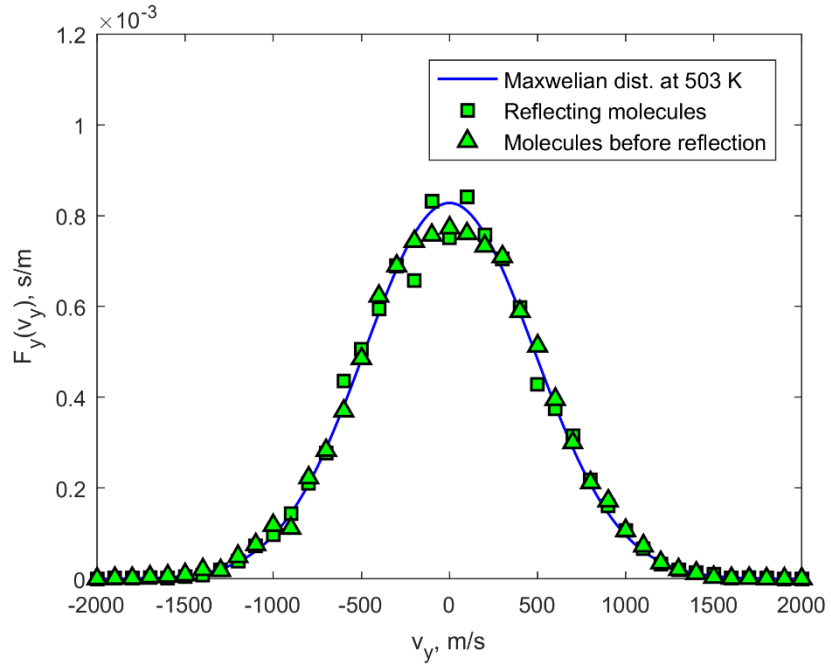

Fig. 30. Velocity distribution function of reflecting molecules in *y* direction.

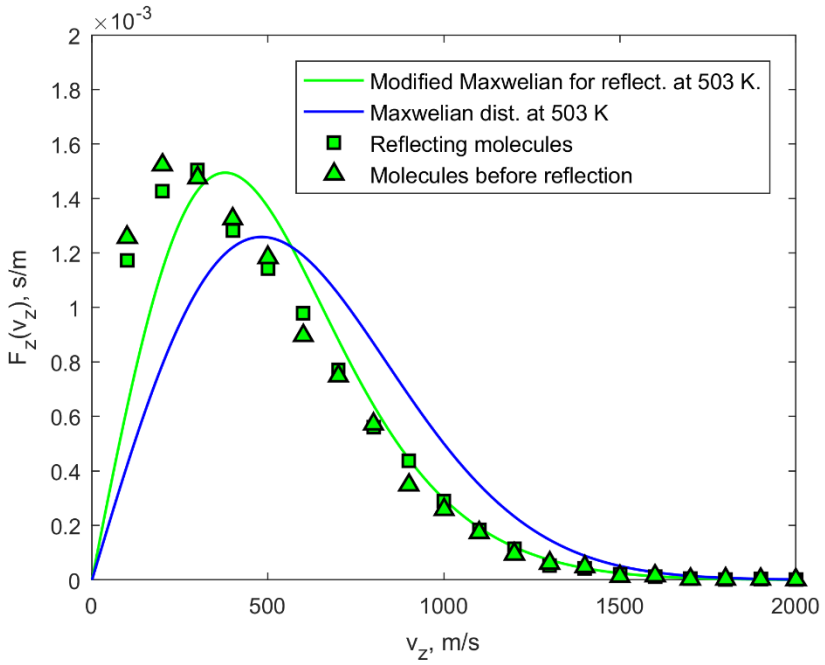

Fig. 31. Velocity distribution function of reflecting molecules in *z* direction.

3.9. Stall times of evaporating condensing and reflecting molecules

The stall time distributions of evaporating, condensing and reflecting molecule are given in Fig. 32. The stall time of the molecule is defined as the time which molecule spends in region between liquid and vapour boundaries before evaporating, condensing or reflecting. It is seen that stall times of evaporating and condensing molecules coincide with each other. Also, the distribution function of stall time increases up to the point of around 12 ps, which is most probable evaporation/condensation stall time, and then the function starts to decrease as stall time increases. The mean stall time of evaporating/condensing molecules is $\bar{t}_{e/c} = 28.00$ ps. On the other hand, the behaviour of stall time probability function is different in case of reflecting molecules: the function decreases with increasing stall time in whole region. The mean stall time of reflecting molecules is considerably shorter and is $\bar{t}_r = 8.93$ ps. Furthermore, the mean free path of water molecules in vapour phase is given by [23]

$$l = \frac{1}{\sqrt{2}\pi\sigma^2(\rho_v/m)} \tag{54}$$

where $\sigma = 2.641$ Å is collision cross-section of water molecule, ρ_v is vapour phase density and m is the mass of water molecule. Since, the value of ρ_v is known from the simulations and the mean translational velocity in vapour phase is given by

$$\bar{v} = \sqrt{\frac{8k_BT}{\pi m}} \tag{55}$$

the mean time between molecular collisions in vapour phase can be evaluated. The mean time in 503 K simulation is $\bar{t} = 20.8\,ps$. It can be seen that most molecules are reflected in shorter times than the $\bar{t}$ and, therefore, these reflections might be result of single-collision processes at the

interphase. The molecules, which are reflected with longer stall times might undergo multiple collisions at the interphase during the reflection.

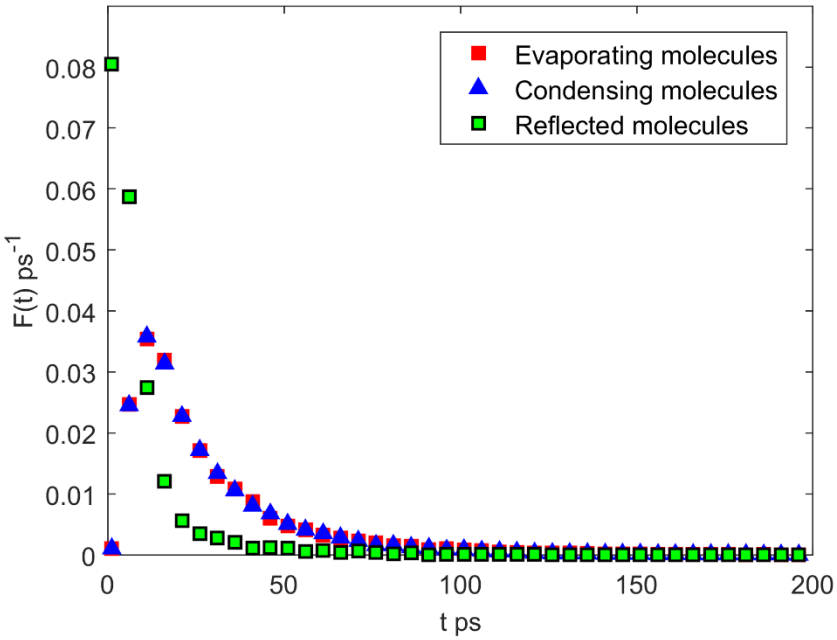

Fig. 32. Stall times of evaporating, condensing and reflecting molecules.

Conclusions

The molecular dynamics simulations of liquid-vapour phase equilibrium state of water were performed using TIP3P, SPC/E and flex-FPC molecular models at five different temperatures: 300 K, 350 K, 400 K, 450 K and 500 K to test the methodology of present master's thesis and to investigate liquid, vapour and interphase properties at equilibrium state. Furthermore, simulations were performed at temperatures: 423 K, 443 K, 463 K, 483 K and 503 K using flex-FPC molecular model in order to investigate the phase change boundary conditions with flexible molecular model of water. From the results of present master's thesis, the following conclusions were drawn:

1. The one over the "10-90" interphase thickness $1/d_{10-90}$ is a decreasing linear function of temperature (given by eq. (43)) in temperature range:

   - from 300 K to 500 K for TIP3P model;
   - from 300 K to 540 K for SPC/E model;
   - from 300 K to 550 K for flexible fixed-point charge model.

   Furthermore, obtained results were compared with TIP4P model results from [15]. The $1/d_{10-90}$ is also linear function of temperature in for TIP4P model, however, it decreases more rapidly for than results obtained in present master's thesis.

2. The condensation coefficient obtained with flex-FPC model is function of liquid temperature T and surface-normal component of translational motion energy E_z of impinging molecule (given by eq. (47)) in temperature range from 443 K to 503 K. The condensation coefficient values of water obtained in present thesis were considerably higher than condensation coefficients from [17], where authors used rigid SPC/E molecular model in similar temperature range. The higher condensation coefficient values for flexible model were obtained due to stabilization process, during which the part of translational motion energy of colliding molecules is transferred to vibrational motion energy. Furthermore, no dependencies of condensation coefficient on surface-tangential components E_x and E_y and energy of rotational motion E_{rot} were observed.

3. The changes of surface-tangential and surface-normal components of translational energy ΔE_x, ΔE_y and ΔE_z and rotational energy ΔE_{rot} of reflected molecules are decreasing linear functions of respective energy components of impinging molecules (given by (49)). Molecules with higher components of energy tend to transfer part of their energy to other forms of energy and to interphase molecules. Therefore, they reflect with lower values of respective energy components. On the other hand, molecules with small energy components undergo a gain of respective energy of these components.

4. The surface-tangential components of translational velocities v_x and v_y of evaporating, condensing and reflecting molecules agree with Maxwellian distribution (given by eq. (50)) at 503 K temperature. However, in velocity interval $v_{x,y} \in [-400; 400]\ m/s$ the values of probability density function for reflecting molecules obtain from simulations slightly scatter due to small number of events sampled during simulations.

5. The mean value of surface-normal component of translational velocity v_z for evaporating molecules is slightly higher than mean velocity obtained from Maxwellian distribution (given by eq. (51)) at 503 K temperature. The value of probability density function of reflecting molecules is higher in lower velocity region and, therefore, whole distribution is shifted to the lower velocities. Furthermore, The modified Maxwellian distributions, which include condensation coefficients obtained in present thesis, for evaporating and reflecting molecules (given by eq. (52) and eq. (53)) give better explanation for the simulation results, however, there still is significant deviation in the case of reflecting molecules.

Reference list

[1] V.P. Singh, C.-Y. Xu, Evaluation and Generalization of 13 Mass-Transfer Equations for Determining Free Water Evaporation, Hydrol. Process. 11 (1997) 311–323. doi:10.1002/(SICI)1099-1085(19970315)11:3<311::AID-HYP446>3.3.CO;2-P.

[2] J. Of, T.H.E. Atmospheric, Temperature Dependence of Evaporation Coefficient for Water Measured in Droplets, J. Atmos. Sci. 64 (2006) 996–1004. doi:10.1175/JAS3860.1.

[3] G. Xue, Y. Xu, T. Ding, J. Li, J. Yin, W. Fei, Y. Cao, J. Yu, L. Yuan, L. Gong, J. Chen, S. Deng, J. Zhou, W. Guo, Water-evaporation-induced electricity with nanostructured carbon materials, Nat. Nanotechnol. 12 (2017) 317–321. doi:10.1038/nnano.2016.300.

[4] A.H. Persad, C.A. Ward, Expressions for the Evaporation and Condensation Coefficients in the Hertz-Knudsen Relation, Chem. Rev. 116 (2016) 7727–7767. doi:10.1021/acs.chemrev.5b00511.

[5] Z. Liang, P. Keblinski, Molecular simulation of steady-state evaporation and condensation in the presence of a non-condensable gas, J. Chem. Phys. 148 (2018). doi:10.1063/1.5020095.

[6] M. Bond, H. Struchtrup, Mean evaporation and condensation coefficients based on energy dependent condensation probability, Phys. Rev. E. 70 (2015) 1–21. doi:10.1103/PhysRevE.70.061605.

[7] R. Marek, J. Straub, Analysis of the evaporation coefficient and the condensation coefficient of water, Int. J. Heat Mass Transf. 44 (2001) 39–53. doi:10.1016/S0017-9310(00)00086-7.

[8] I.W. Eames, N.J. Marr, H. Sabir, The evaporation coefficient of water: A review, Int. J. Heat Mass Transf. 40 (1997) 2963–2973. doi:10.1016/S0017-9310(96)00339-0.

[9] K. Almenas, Evaporation/Condensation of Water: Unresolved Issues − I. Phase Change at Low Pressures, Laminar Conditions, Versus aureus, Kaunas, 2015.

[10] M. Kulmala, P.E. Wagner, Mass accommodation and uptake coefficients - A quantitative comparison, J. Aerosol Sci. 32 (2001) 833–841. doi:10.1016/S0021-8502(00)00116-6.

[11] Accommodation coefficient, (n.d.). http://www.thermopedia.com/content/286/.

[12] R.A. Shaw, D. Lamb, Experimental determination of the thermal accommodation and condensation coefficients of water, J. Chem. Phys. 111 (1999) 10659–10663. doi:10.1063/1.480419.

[13] T. Tsuruta, A. Tokunaga, G. Nagayama, Molecular Boundary Conditions and Accommodation Coefficient on A Nonequilibrium Liquid Surface, 27th Int. Symp. Rarefied Gas Dyn. 1333 (2011) 859–864. doi:10.1063/1.3562753.

[14] G.S. Hwang, M. Kaviany, Molecular dynamics simulation of effective thermal conductivity of vapor-filled nanogap and nanocavity, J. Appl. Phys. 106 (2009). doi:10.1063/1.3186043.

[15] T.H. Yang, C. Pan, Molecular dynamics simulation of a thin water layer evaporation and evaporation coefficient, Int. J. Heat Mass Transf. 48 (2005) 3516–3526. doi:10.1016/j.ijheatmasstransfer.2005.03.015.

[16] T. Tsuruta, H. Tanaka, T. Masuoka, Condensation-evaporation coefficient and velocity distributions at liquid–vapor interface, Int. J. Heat Mass Transf. 42 (1999) 4107–4116. doi:https://doi.org/10.1016/S0017-9310(99)00081-2.

[17] T. Tsuruta, G. Nagayama, Molecular Dynamics Studies on the Condensation Coefficient of Water, J. Phys. Chem. B. 108 (2004) 1736–1743. doi:10.1021/jp035885q.

[18] Y.W. Wu, C. Pan, Molecular Dynamics Simulation of Evaporation of a Thin Liquid Argon Layer in a Closed System, ASME Summer Heat Transf. Conf. (2003) 1–4.

doi:10.1115/HT2003-47217.

[19] G. Nagayama, M. Kawagoe, T. Tsuruta, Molecular Dynamics Simulations of Interfatial Heat and Mass Transfer at Nanostructured Surface, 2007 First Int. Conf. Integr. Commer. Micro Nanosyst. (2016). doi:10.1115/MNC2007-21410.

[20] G. Nagayama, M. Kawagoe, A. Tokunaga, T. Tsuruta, On the evaporation rate of ultra-thin liquid film at the nanostructured surface : A molecular dynamics study, Int. J. Therm. Sci. 49 (2010) 59–66. doi:10.1016/j.ijthermalsci.2009.06.001.

[21] G. Nagayama, M. Takematsu, H. Mizuguchi, T. Tsuruta, G. Nagayama, M. Takematsu, H. Mizuguchi, T. Tsuruta, Molecular dynamics study on condensation/evaporation coefficients of chain molecules at liquid – vapor interface, J. Chem. Phys. 143 (2015). doi:10.1063/1.4923261.

[22] T. Ishiyama, T. Yano, S. Fujikawa, Molecular dynamics study of kinetic boundary condition at an interface between argon vapor and its condensed phase, Phys. Fluids. 16 (2004). doi:10.1063/1.1763936.

[23] T. Ishiyama, T. Yano, S. Fujikawa, Molecular dynamics study of kinetic boundary condition at an interface between a polyatomic vapor and its condensed phase, Phys. Fluids. 16 (2004) 4713–4727. doi:10.1063/1.1811674.

[24] T. Ishiyama, T. Yano, S. Fujikawa, Molecular dynamics study on the evaporation part of the kinetic boundary condition at the interface between water and water vapor, Rafefied Gas Dyn. 24-Th Int. Symp. (2005) 491–497. doi:10.1063/1.1941584.

[25] K. Kobayashi, K. Hori, M. Kon, K. Sasaki, Molecular dynamics study on evaporation and reflection of monatomic molecules to construct kinetic boundary condition in vapor – liquid equilibria, Heat Mass Transf. 52 (2015) 1851–1859. doi:10.1007/s00231-015-1700-6.

[26] M. Kon, K. Kobayashi, M. Watanabe, Molecular Simulation of Evaporation Mass Flux during Net Evaporation / Condensation, 30th Int. Symp. Rarefied Gas Dyn. 1786 (2016). doi:10.1063/1.4967621.

[27] M. Kon, K. Kobayashi, M. Watanabe, Kinetic boundary condition in vapor–liquid two-phase system during unsteady net evaporation/condensation, Eur. J. Mech. B/Fluids. 64 (2017) 81–92. doi:10.1016/j.euromechflu.2016.12.001.

[28] K. Kobayashi, K. Sasaki, M. Kon, H. Fujii, Kinetic boundary conditions for vapor – gas binary mixture, Microfluid. Nanofluidics. 21 (2017). doi:10.1007/s10404-017-1887-6.

[29] K. Kobayashi, K. Sasaki, M. Kon, H. Fujii, M. Watanabe, Molecular Dynamics Simulation on Kinetic Boundary Conditions of Gas-Vapor Binary Mixture, 30th Int. Symp. Rarefied Gas Dyn. 110002 (2016). doi:10.1063/1.4967622.

[30] J. Julin, M. Shiraiwa, R.E.H. Miles, J.P. Reid, U. Po, Mass Accommodation of Water : Bridging the Gap Between Molecular Dynamics Simulations and Kinetic Condensation Models, J. Phys. Chem. A. 117 (2013). doi:10.1021/jp310594e.

[31] P. Louden, R. Schoenborn, C.P. Lawrence, Fluid Phase Equilibria Molecular dynamics simulations of the condensation coefficient of water, Fluid Phase Equilib. 349 (2013) 83–86. doi:10.1016/j.fluid.2013.04.006.

[32] I. Napari, H. Vehkamäki, A comparison of rigid and flexible water models in collisions of monomers and small clusters, J. Chem. Phys. 125 (2006) 1–7. doi:10.1063/1.2346674.

[33] X.B. Zhang, Q.L. Liu, A.M. Zhu, An improved fully flexible fixed-point charges model for water from ambient to supercritical condition, Fluid Phase Equilib. 262 (2007) 210–216. doi:10.1016/j.fluid.2007.09.005.

[34] D. Frenkel, B. Smit, Understanding Molecular Simulation - From Algorithms to Applications, Academic Press, 2002.

[35] Linked-List Cell Molecular Dynamics, (n.d.) 1–3.

[36] M. Dobson, I. Fox, A. Saracino, Cell list algorithms for nonequilibrium molecular dynamics, J. Comput. Phys. 315 (2016) 211–220. doi:10.1016/j.jcp.2016.03.056.

[37] Constructing a neighbour list, (2015) 1–19.

[38] C.U.I. Zhiwei, S.U.N. Yi, Q.U. Jianmin, The neighbor list algorithm for a parallelepiped box in molecular dynamics simulations, (2009) 0–7. doi:10.1007/s11434-009-0197-0.

[39] W. Li, T. Ying, W. Jian, D. Yu, Comparison research on the neighbor list algorithms : Verlet table and linked-cell, Comput. Phys. Commun. 181 (2010) 1682–1686. doi:10.1016/j.cpc.2010.06.005.

[40] D. Frenkel, B. Smit, Understanding Molecular Simulation: From Algorithms to Applications, Second, Academic Press, San Diego, 2002.

[41] A. Džiugys, B. Peters, An approach to simulate the motion of spherical and non-spherical fuel particles in combustion chambers, Granul. Matter. 3 (2001) 231–266. doi:10.1007/PL00010918.

[42] M. Fyta, Water models in classical simulations, (n.d.). https://www.icp.uni-stuttgart.de/~icp/mediawiki/images/b/bd/SimmethodsII_ss18_lecture5slides.pdf.

[43] W.L. Jorgensen, J. Chandrasekhar, J.D. Madura, R.W. Impey, M.L. Klein, W.L. Jorgensen, J. Chandrasekhar, J.D. Madura, R.W. Impey, M.L. Klein, Comparison of simple potential functions for simulating liquid water Comparison of simple potential functions for simulating liquid water, 926 (1983). doi:10.1063/1.445869.

[44] P. Taylor, A. Mudi, C. Chakravarty, Effect of the Berendsen thermostat on the dynamical properties of water, Mol. Phys. 102 (2006). doi:10.1080/00268970410001698937.

[45] N. Shuichi, Constant Temperature Molecular Dynamics Methods, Prog. Theor. Phys. Suppl. 103 (1991). doi:https://doi.org/10.1143/PTPS.103.1.

[46] H.J.C. Berendsen, J.P.M. Postma, W.F. Van Gunsteren, A. Dinola, J.R. Haak, H.J.C. Berendsen, J.P.M. Postma, W.F. Van Gunsteren, A. Dinola, J.R. Haak, Molecular dynamics with coupling to an external bath, The Journa. 81 (1984). doi:10.1063/1.448118.

[47] B. Shi, S. Sinha, V.K. Dhir, Molecular dynamics simulation of the density and surface tension of water by particle- particle particle-mesh method Molecular dynamics simulation of the density and surface tension of water by particle-particle particle-mesh method, J. Chem. Phys. 124 (2012) 2006. doi:10.1063/1.2199849.

[48] W.C. Reynolds, Thermodynamic Properties in SI, Department of Mechanical Engineering, Standford, 1979.

[49] D.J. Tobias, N. Sengupta, J.K. Beattie, A.M. Djerdjev, G. Gregory, O. Link, E. Vöhringer-martinez, Y. Liu, K. Siefermann, A.P. Willard, D. Chandler, What ice can teach us about water interactions: a critical comparison of the performance of different water models, Faraday Discuss. 141 (2009). doi:10.1039/b816684f.

[50] J. Alejandre, D.J. Tildesley, G.A. Chapela, G.A. Chapela, Molecular dynamics simulation of the orthobaric densities and surface tension of water Molecular dynamics simulation of the orthobaric densities and surface tension of water, 4574 (1995). doi:10.1063/1.469505.